UNITED NATIONS UNIVERSITY

GEOTHERMAL TRAINING PROGRAMME
Orkustofnun, Grensasvegur 9,
IS-108 Reykjavik, Iceland

Reports 2013
Number 33

SYNTHESIS OF WELL TEST DATA AND MODELLING OF OLKARIA SOUTH EAST PRODUCTION FIELD

Daniel S. Saitet
Kenya Electricity Generating Company, Ltd. – KenGen
Olkaria Geothermal Project
P.O. Box 785-20117, Naivasha,
KENYA
dsaitet@kengen.co.ke

ABSTRACT

Well data was analysed and reservoir parameters were interpreted, then the two were unified, incorporating the entirety of the known knowledge and information into a single simplified conceptual model. The analysed wells are highly permeable with convective zones appearing below 1 km depth in the zone immediately adjacent to Ololbutot lava flow. No independent magmatic heat sources were interpreted for the system, rather NW-SE and NNE-SSE trending faults act as fluid conduits, allowing the fluid to percolate into the deep reservoir rock where it collects heat, and upwells where localized upflow zones, in the vicinity of Well OW-802, appear along permeable structures. The HOLA well bore simulator is used to predict well output curves for deep wells in the field. Most of the wells are fed by a single phase liquid reservoir; therefore, low outputs are expected. A resource assessment was carried out using the Monte Carlo simulation which showed average power output was likely to be produced in the area, about 42 MWe, and the maximum possible output was shown to be in the region of 73 MWe, using conventional flash power plant cycles. A natural state model for the field was constructed using TOUGH2. The model places plausible resource prospect areas along known structures in the area.

1. INTRODUCTION

Olkaria, a large volcanic complex, located at the axis of the Great East African Rift Valley, has been the focus of geothermal exploration in Kenya for many years. Reconnaissance studies were commissioned to explore the area for geothermal resources in the early fifties. Numerous surface manifestations that are prevalent in the area, including fumaroles, altered grounds and sulphur deposits, are believed to have attracted initial explorers to the area. It was not until 1956 that drilling started in the area. Two wells, Wells OW-X1 and OW-X2, were drilled to 950 m depth with no success. The two wells were located close to an area which was most probably easily accessible and with great surface activity. Their failure to sustain discharge discouraged further drilling activity until the oil crisis when exploration for alternative energy sources gathered momentum. By this time, the government and the United Nations Development Program entered into cooperation to support additional exploration studies. Extensive geo-scientific studies were carried out and proved the existence of exploitable resources at Olkaria.

The next well, located southeast of Olkaria Hill, was drilled to a kilometre depth. Well OW-1 was not able to discharge despite being located in a geologically plausible location at the intersection of two major faults. A decision was then made to concentrate drilling efforts eastwards near the most recent lava flow. Well OW-2 was drilled next with great success. The well encountered temperatures above 280°C and discharged high enthalpy fluids. Deep exploration wells were drilled thereafter near this well and culminated in the commission of a 45 MWe plant at Olkaria 1, which was fully operational by 1985.

For further development in the area, a decision was reached to subdivide the large field into seven sectors namely: Olkaria West (OWPF), Olkaria North West (ONWPF), Olkaria Central (OCPF), Olkaria North East (ONEPF), Olkaria East (OEPF), Olkaria South East (OSEPF) production fields and Olkaria Domes. The locations of the field sectors (Figure 1) were decided relative to Olkaria Hill.

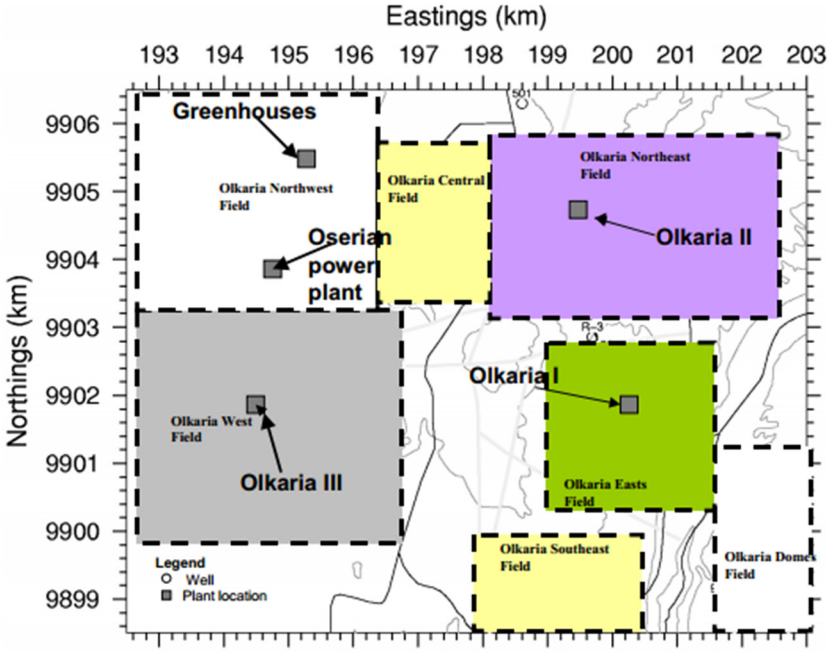

FIGURE 1: Olkaria geothermal field showing seven production sectors

Further drilling activities were concentrated in the Olkaria West and Northeast fields where power plants with 84 MWe and 105 MWe were subsequently built. Drilling at Olkaria Domes did not start until 1998 when the first well was drilled there. To date, many wells have been drilled in the Domes field and a power plant is presently under construction.

Olkaria South East is the subject of this work. Prior to drilling deep wells, the area was thought to be an outflow zone (Ouma, 2009) from the nearby Olkaria East field and, therefore, was somewhat ignored in the exploration for high-temperature geothermal resources. A decision to re-inject hot brine from the Olkaria East production field into this area was also envisaged more recently. To this end, two shallow re-injection wells were drilled near unproductive Well OW-801. These wells were meant to be used in case sites for re-injection near the field were either unavailable or as part of a dynamic reinjection plan, envisaged to become necessary upon completion of an additional 140 MW power plant which is also under construction.

However, recent deep drilling, commenced with the drilling of Well OW-802, revealed that this field could be productive. Well OW-11A, drilled from the Olkaria East production field, directed under the Ololbutot lava flow, turned out to be very impressive. More wells have now been sited and drilled in the area, all giving positive results. It is unfortunate that, to date, none of these wells has been flow tested. It is expected that further appraisal drilling will continue in this area, at least in the near future, before current wells can be flow tested. A critical review of available data is, therefore, necessary if drilling is to continue.

This project, consequently, is focussed on synthesising available well test data to attempt to understand the properties, geometry and nature of the reservoir there. This work, apart from attempting to model reservoir conditions at depth, is also aimed at estimating the productivity of the wells already drilled and the resource capacity.

2. GEOLOGY AND STRUCTURAL SETTING

2.1 Geological setting

Olkaria is located at the floor of the central Kenyan Rift about 150 km northeast of Nairobi. The area is both geologically and structurally complex. The volcanic system is associated with an old central volcano which collapsed, leaving a large caldera rim of approximately 5 km which is defined, in part, by a ring fracture and by pumice domes. Rocks occurring on the surface are predominantly quaternary comendites, pumice fall and ash deposits of late Pliocene to Holocene. Some trachytic flows appear to the south of the geothermal area below thick pyroclastic covers associated with Longonot and Suswa eruptive material. Minor volcanic glass material also appears in a few localities.

Volcanic centres are structurally controlled. The main eruptive centre is the Olkaria hill, with major structural features contributing significantly. The Ololbutot and Gorge farm faults are such eruptive fissures. The most recent volcanic episode is associated with the Ololbutot fault which produced rhyolite flows dated about 250 years BP, based on charred wood found under it (Clarke et al., 1990).

The lithostratigraphic structure in the area is nearly horizontal (Muchemi, 1999; and Brown, 1984). Based on rock cutting and cores, the general lithostratigraphy of the greater Olkaria complex can be divided into two, with the axis separating the western sector from the eastern sector passing through Olkaria hill. Omenda (1998) discussed these formations and proposed nomenclature: Mau tuffs, Plateau trachytes, Olkaria basalts and Upper Olkaria volcanics. Mau tuffs were found to be unique to the western sector, while the trachytes and basalts are unique to the eastern sector.

Geothermal manifestations are structurally controlled. Hot grounds and fumaroles are located along fractures, with intense activity found at their intersections. Production wells sited at these intersections prove to be particularly good.

2.2 Structures

Olkaria is a complex grid faulted area located in the vicinity of western rift boundary faults of the Rift system. Tectonic activity is associated with extensional rifting and consequent tension created North-South faulting along the axis of the rift. The dominant structures at Olkaria are the Ololbutot fault (North-South), the Gorge farm fault (North East-South West), the Olkaria Fault (East North East-West South West) and the Suswa fault (North East-South West). An alignment of eruptive domes is prominent to the east of the field, probably demarcating a caldera rim, and was mapped elsewhere around the greater volcanic complex. Many other buried faults with similar trends have been inferred by analysis of drill cores and rock cuttings. (Muchemi, 1998; Omenda, 1998). Micro-seismic monitoring of Olkaria geothermal field showed lineaments of epicentres similar to mapped structures (Simiyu and Keller, 1999). Intersections of these lineaments are associated with shallower and less prominent seismic events suspected to be consequent to fluid flow in the subsurface.

Olkaria South East field (OSEPF) is traversed by the Ololbutot fault to the west, a North West-South East trending fault passing through the Ololbutot recent lava flow, and is bounded to the east by the Olchorro Oirowua gorge. Another prominent structure trends NNE-SSW, intersecting with NW-SE fault in close vicinity to Well OW-804 in the OSEPF. A shorter parallel fault is also intersected by Wells OW-804A and OW-802A which were drilled directionally to the southeast. The inferred alignment of eruptive centres offers a natural boundary for the field to the south. The field is juxtaposed with the Olkaria East production field, which has produced for more than 30 years, and the Domes field, which is currently in the development phase. Figure 2 shows the structural map of the greater Olkaria geothermal field.

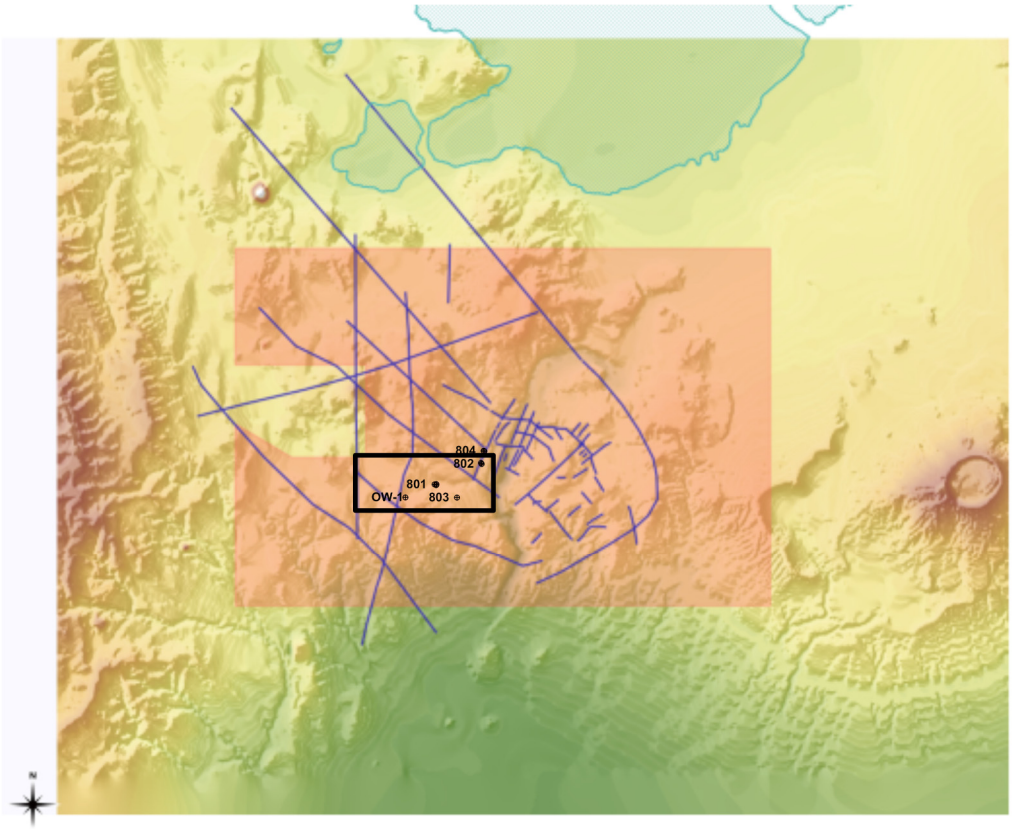

FIGURE 2: Structural map of Olkaria geothermal field; inset is the Olkaria Southeast production field; black dots show locations of drilled wells

3. ANALYSIS OF TEMPERATURE AND PRESSURE PROFILES

Drilling involves pumping large volumes of cold water or air into a well for a long time. This destabilizes the thermodynamic conditions of a well and the formations in the near vicinity. After geothermal wells are completed, temperature and pressure profiles are taken during warm-up. Temperature measured in the well during the period of thermal recovery is useful in determining feed zones of the well, physical conditions such as boiling, head transfer mechanisms, fluid flow patterns and in estimating formation temperatures of the undisturbed reservoir. However, it is important to note that drilling does change the conditions of the reservoir such that we can never know the exact initial prevailing conditions. The feed zones in the well tend to accept drilling fluids, thus cooling them significantly and these feed zones will, consequently, recover more slowly than their surroundings. Profiles, taken while injecting fluids into the well, show these points as fluid loss zones, represented by rapid changes in the thermal gradient. Later, as the well recovers from drilling effects, such changes in thermal gradients are associated with aquifer feed points.

An important aspect in the analysis of temperature profiles is the determination of the physical conditions and processes occurring in the well and its immediate surroundings. In determining the physical conditions of the well fluid, it is obviously important to determine the boiling conditions. In the case of high temperature wells, the question of whether boiling processes occur in the well or in the reservoir is answered. Boiling temperature increases with increases in pressure. Fluids at greater depth are, therefore, expected to boil at higher temperatures. In evaluating estimated boiling temperatures, the effects of salinity and impurities in the water are ignored. In ICEBOX, a program called Boilcurv is available for finding the boiling point with depth curve. The program computes the boiling point curve

from a reference pressure provided by the user, based on the integral formula of pressure (Equation 1) that follows the water saturation density with depth (Arason et al., 2004).

$$P(z) = P_o + g\int \rho_{sat}(P(z))dz \quad \textbf{(1)}$$

where $P(z)$ = Pressure at any depth;
P_o = Pressure at initial elevation;
ρ_{sat} = Density in a column of single phase fluid at saturation pressure;
g = Gravitational acceleration;
z = Depth.

Thermal transfer mechanisms in the well are identifiable from temperature profiles. Essentially, only conduction and convective heat transfer occur in geothermal wells. The two mechanisms are easily identifiable in geothermal wells. Conductive heat transfer is commonly represented by high gradient profiles in a straight line in impermeable rock formations. In contrast, convective heat transfer manifests when temperature profiles show isothermal conditions at small to greater depths. This usually results in vertical temperature profiles. Convection is very important in geothermal studies as it points out permeability in geothermal reservoirs. Identifying areas with conduction and convection heat transfer is very important in identifying the components of the reservoir. The cap rock is commonly dominated by conduction with a steep gradient while convective zones denote the reservoir. Obviously, wells should be cased at the reservoir to avoid the incursion of colder fluids.

Using the temperatures recorded during the warm-up period, one is able to estimate formation temperatures. In some cases, it involves fitting a curve to later profiles if the temperature stabilizes over a reasonably long time. Some wells stabilize in temperature rather quickly. In many cases, two phase well conditions may follow the boiling point curve. Semi analytical methods are available today for better estimation of these temperatures. There are two widely used methods for doing this. The Horner method (Dowdle and Cobb, 1975; Takai et al., 1994) and the Albright method (Albright, 1976).The Albright method is useful for short term heating such as in determining formation temperature during drilling for blow out prevention. The Horner method is more appropriate for longer heating up periods, such as when a well is warming up after drilling. Temperatures recorded at a point for different warm-up times are plotted against the Horner time and a line is fitted to the points whose extrapolation to long times gives the estimate of the formation temperature. It is important to fit the straight line to latter points when it is expected that the well has somewhat approached full recovery. Arason et al. (2004) presented a robust software, Berghiti, included in ICEBOX, for performing this task.

Pressure in the reservoir is directly related to the reservoir fluid. It is the reservoir fluid that mines and transports the heat that is present in the rock to the surface. Its importance cannot, therefore, be over-emphasised. Pressure gradients are the driving forces for fluid flow in the reservoir. Pressure gradient in a flowing geothermal well can be described by three terms (Equation 2). The first term is associated with frictional forces as the fluid travels up the well; the second is associated with acceleration of the fluid; and the last term is due to the pressure potential. In hydrostatic wells, only the third term is non-zero.

$$\frac{dP}{dz} = \left[\frac{dP}{dz}\right]\text{fric} + \left[\frac{dP}{dz}\right]\text{acc} + \left[\frac{dP}{dz}\right]\text{pot} \quad (2)$$

where P = Pressure;
z = Depth.

Pressure changes during warm up as fluid becomes lighter, and the pressure profiles are expected to revolve around a point of constant reservoir pressure known as the "best feedzone''. This point is commonly referred to as the pivot point and is the best connection to the reservoir, representing reservoir pressure at that depth. Pressure is stable here since the volume concerned is ideally very big; therefore, heating does not result in significant density variations. The method employed to evaluate initial

formation pressure involves calculating a hydrostatic profile based on a formation temperature profile and then fitting the so calculated hydrostatic pressure profile through the pivot point observed during warm up. In this work, the program Predyp, presented by Arason et al. (2004) was used to calculate the initial pressure from estimated formation temperature profiles.

3.1 Heat-up profiles

Well OW-1 was the first well drilled in the UNDP project of 1975 after unsuccessful attempts at the initial two sites much earlier. It is located in the vicinity of two intersecting fault zones in an area dominated by intense surface activity. Well OW-1 was drilled to a depth of 1003 m, reaching temperatures of 126°C at the bottom. This well was abandoned without a wellhead valve and is still open to the atmosphere. Vertical permeability is evident in this area, especially slightly east of Well OW-1 where fumarolic activity is most intense. No pressure measurements were recorded in this well.

Well OW-801 was drilled near the Ololbutot lava flow in 1996. It is assumed that this well has equilibrated with formation conditions after about 8 years of heating up. The well intersected vertical flows of fluid of more than 200°C from about 1300 m depth to the bottom (2000 m), where it achieves a stable temperature of 215°C (Figure 3a). With the casing set at 847 m depth, the well feed point is located at 950 m where colder inflows are expected; minor ones are found at 1350 m. This well is, therefore, unproductive and has no wellhead pressure. No boiling occurs in the well. The pressure profiles (Figure 3b) are hydrostatic and show the water level at 575 m depth.

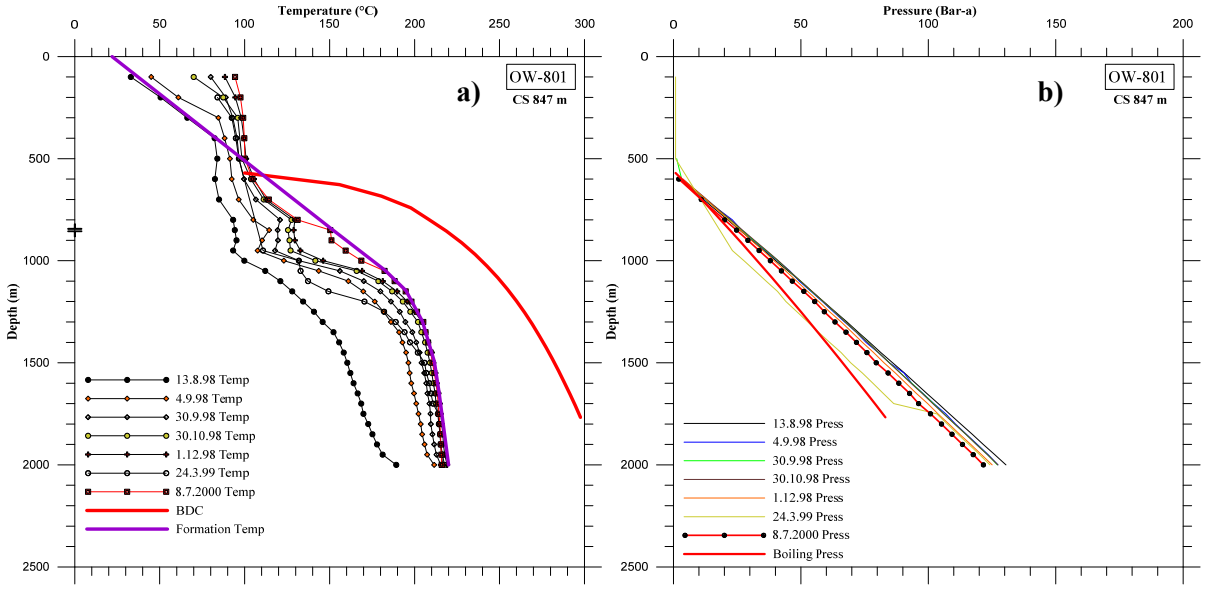

FIGURE 3: Well OW-801: a) Temperature profiles; b) Pressure profiles

Wells OW-801R1 and OW-801R2. Two shallow wells were drilled on Well OW-801's well pad, originally meant for possible shallow reinjection. These wells are located side by side at 50 m separation. The temperature profiles (Figures 4a) in Well OW-801R1 show a cold well cased at 190 m with feed points at 300, 350 and 500 m. The main feed zone was interpreted to be at 350 m. The well was drilled to 600 m, achieving about 90°C at the bottom, measured after twenty days of heating up. Similarly, Well OW-801R2 (Figures 5a) intersects permeable feed points at 350, 500 and 550 m. The well is cased at 266.7 m depth and reached 103°C at the bottom (640 m) after thirty three days of heating up. Pressure profiles for Well OW-801R1 (Figure 4b) and Well OW-801R2 (Figure 5b) are predominantly hydrostatic, with water levels located at 370 and 520 m, respectively, based on the latest profiles.

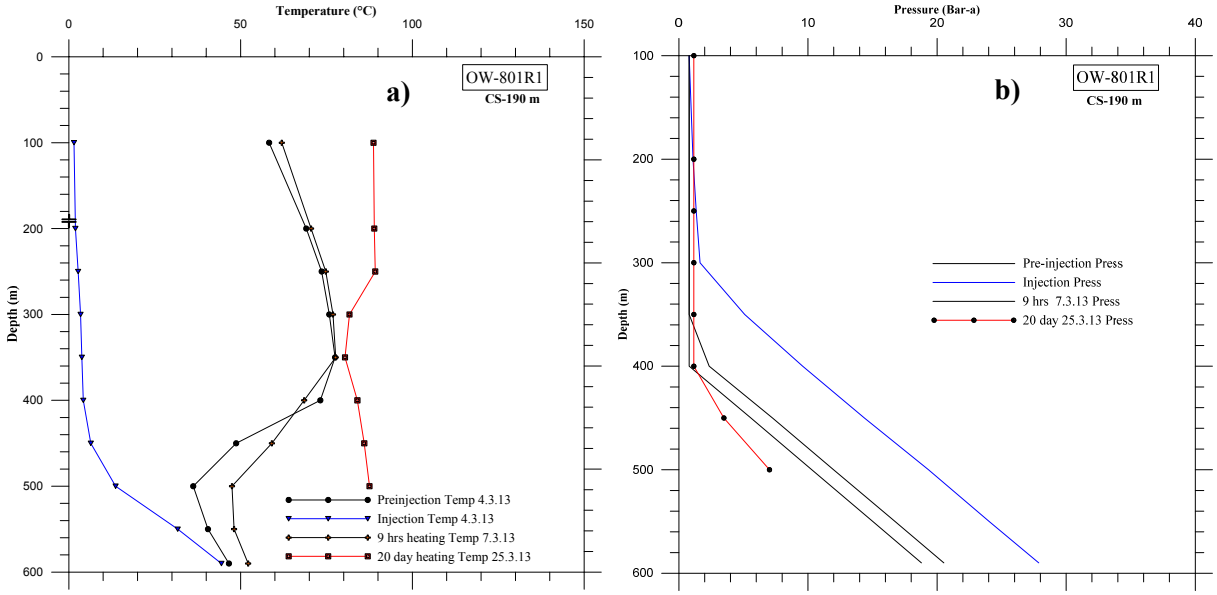

FIGURE 4: Well OW-801R1: a) Temperature profiles; b) Pressure profiles

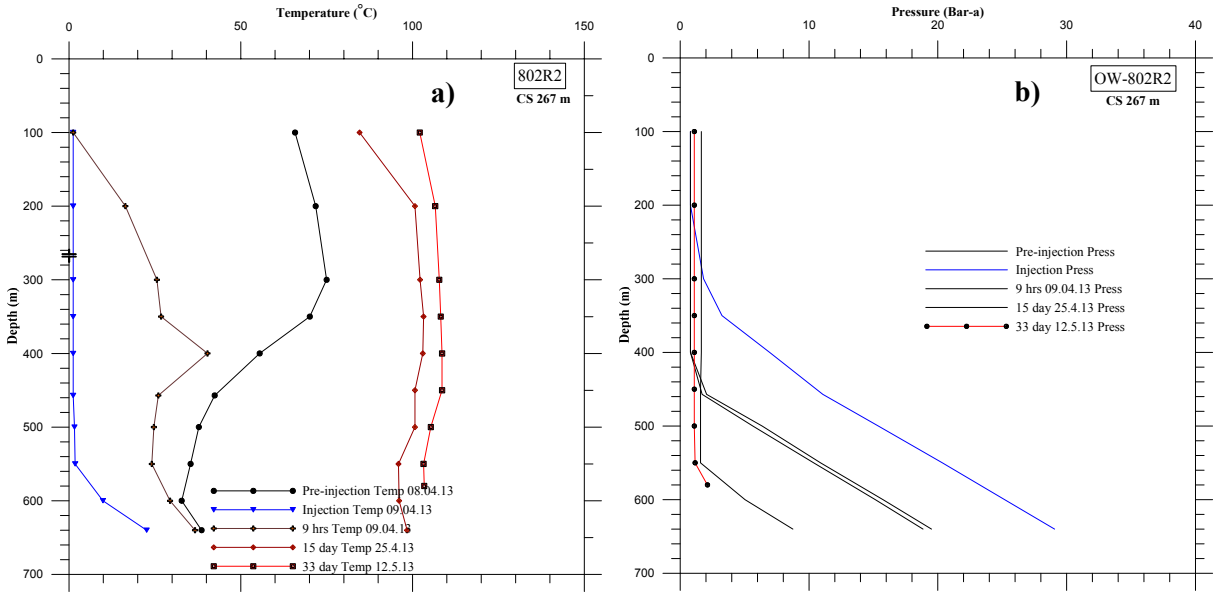

FIGURE 5: Well OW-801R2: a) Temperature profiles; b) Pressure profiles

Well OW-802, drilled to 3000 m depth, intercepted hot aquifers at 850, 1050, 1800 and 2000 m with cross flows between them. The temperature (Figure 6a) reached about 280°C at the bottom of the well. The best feed zone was estimated to be at 1050 m. Boiling occurs inside the well at 1300 m depth. Pressure profiles (Figure 6b), taken for up to 144 days of heating, show the pressure pivot point in the region of 1150 m depth. The latest profile indicates possible wellhead pressures of 33.1 bar-g down from 170 bar at the well bottom.

Well OW-802A was drilled directionally (N137°E) to a depth of 3000 m and intercepts hot aquifers at 850, 1800 and 2500 m (Figure 7a). The main aquifer intersected by Well OW-802 is located at about 1800 m in this well and contributes a significant part of fluid into the well at about 237°C. Later temperature measurements appear to approximate near vertical isotherms increasingly heating up. Boling occurs just above the casing depth. The formation temperature follows the shape of the boiling

point temperature. Pressure profiles (Figure 7b) show 200 bar-a at the bottom and suggest 28.2 bar-g can be expected at the well top and a hydrostatic level at 500 m. A unique and prominent pressure control point is not clear in this well. However, a pivot point is suggested at 1500 m depth.

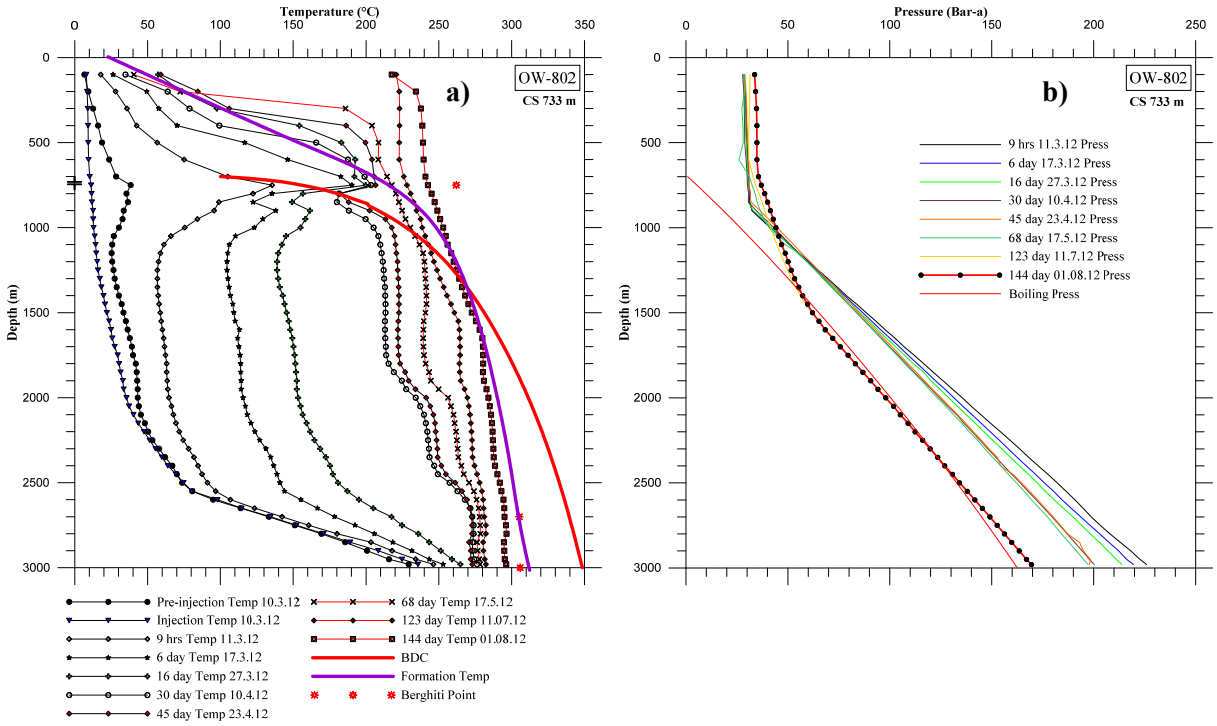

FIGURE 6: Well OW-802: a) Temperature profiles; b) Pressure profiles

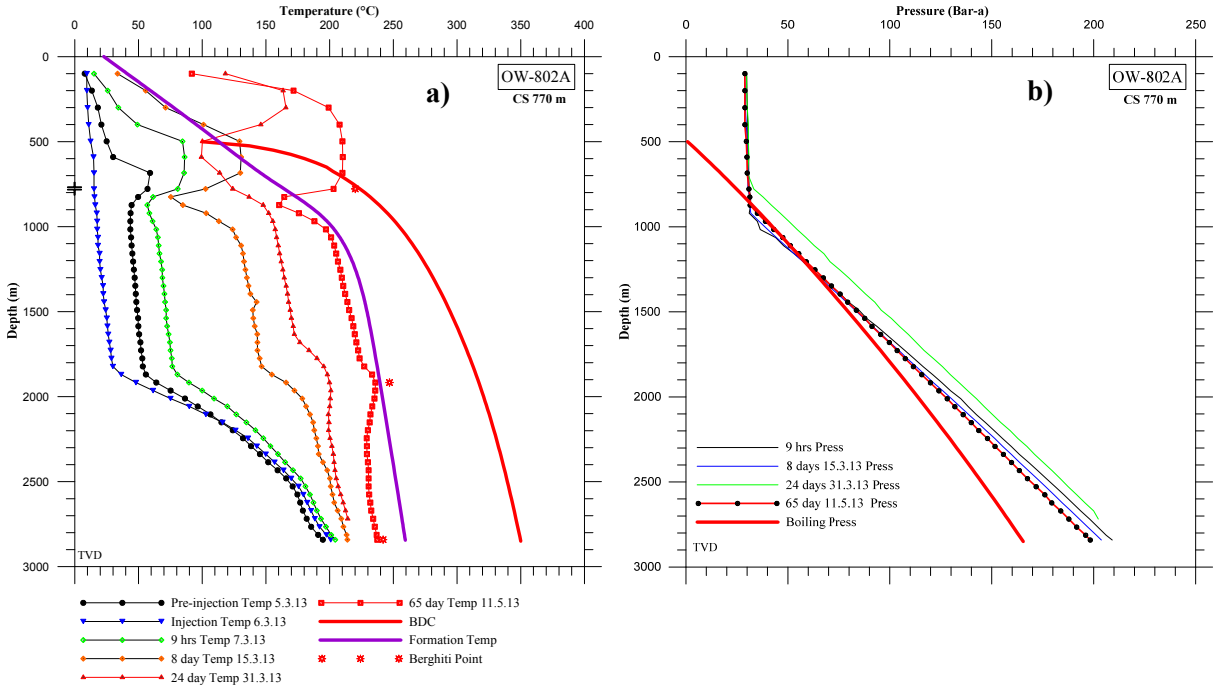

FIGURE 7: Well OW-802A: a) Temperature profiles; b) Pressure profiles

Well OW-803. In this well, feed points are located at 1300, 1500, 1800, 2500 and 2850 m, delivering fluids of about 230°C after about three months of heating up (Figure 8a). The formation temperature

follows the boiling point curve. A temperature reversal occurs near the bottom and is attributable to a bottom feedzone that is slowly recovering from the effects of drilling. Eventually, this effect is expected to disappear as stable formation temperatures are reached. Pressure profiles (Figure 8b) taken in this well show a non-artesian well with a hydrostatic level at 575 m with pressure profiles slowly revolving around 1500 m depth where a pivot point is located. The well reaches pressures above 200 bar-a at the bottom.

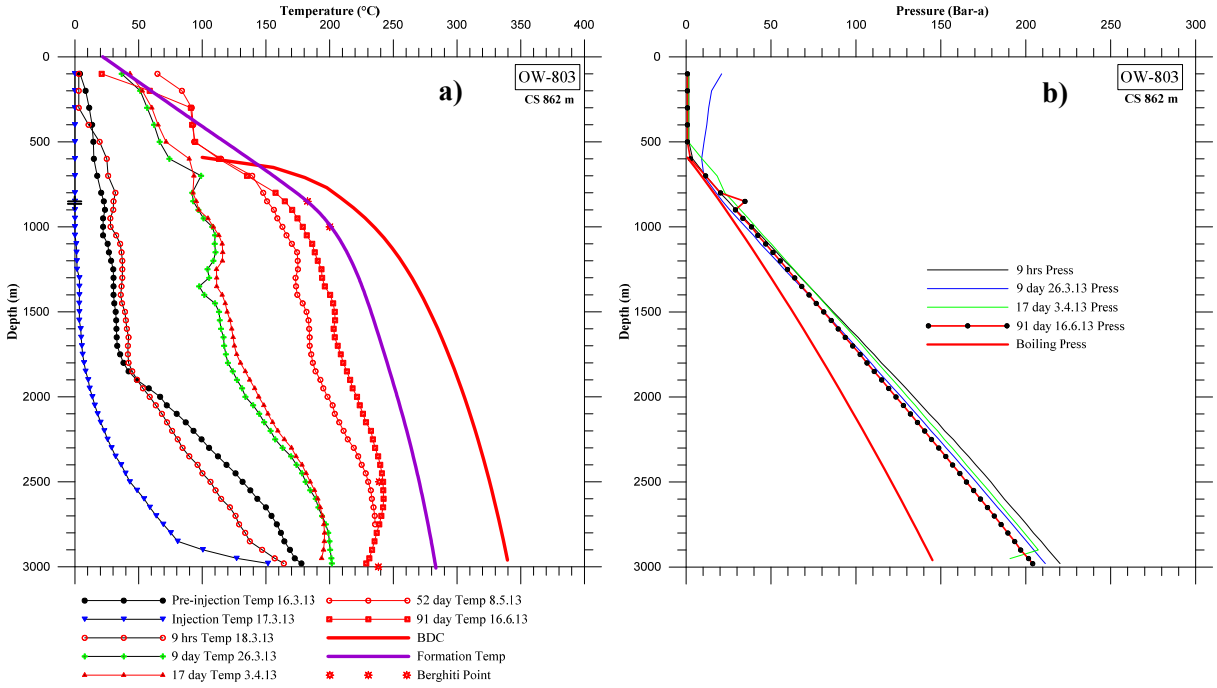

FIGURE 8: Well OW-803: a) Temperature profiles; b) Pressure profiles

Well OW-804 is the hottest well in this field at present. The well intersects hot feeder zones at 850, 1500, 1900, 2200 and 2900 m and reaches temperatures over 300°C at the bottom (Figure 9a). Gas pressure accumulates at the well's top and as steam condenses, as evidenced by drastic cooling in the shallower cased off regions. Most of the reservoir is shown to be a vertical isotherm of 250°C which shifts closer to 300°C towards the final one third of the well. In determining the boiling temperature in this well, the pressure profile was used to calculate the corresponding boiling temperature. Pressure profiles (Figure 9b) collected from this were not consistent with the temperature, as the tool was reported to leak or fail completely. Consequently, these measurements were dropped from this analysis. Initial pressures taken just after drilling showed higher pressures at the bottom, which eventually even out to about 140 bar-a after 75 days of heating up. It is difficult to evaluate a pivot point with so few pressure profiles. However, a depth of 1200 m is suggested by available data.

Well OW-804A is directionally drilled (N145°E) and intersects hot feed zones at 1200, 1300, 1450, 2250 and 2450 m with relative contribution probably highest at 2250 m. The formation temperature follows the boiling point temperature with flashing occurring only inside the casing, and reaches over 310°C at the bottom (Figure 10a). Pressure profiles (Figure 10b) show a hydrostatic level at 575 m depth. The well bottom is at 150 bar-a pressure, and 31 bar-g is expected at the wellhead.

3.1.1 Summary

Feedzones:
Table 1 summarizes the temperature situation in all the wells in this field as well as feed zone locations. Wells OW-802, OW-804 and OW-804A encounter temperatures above 280°C while Wells OW-802A and OW-803 reached temperatures in the range of 230-240°C for the latest measured bottom-hole

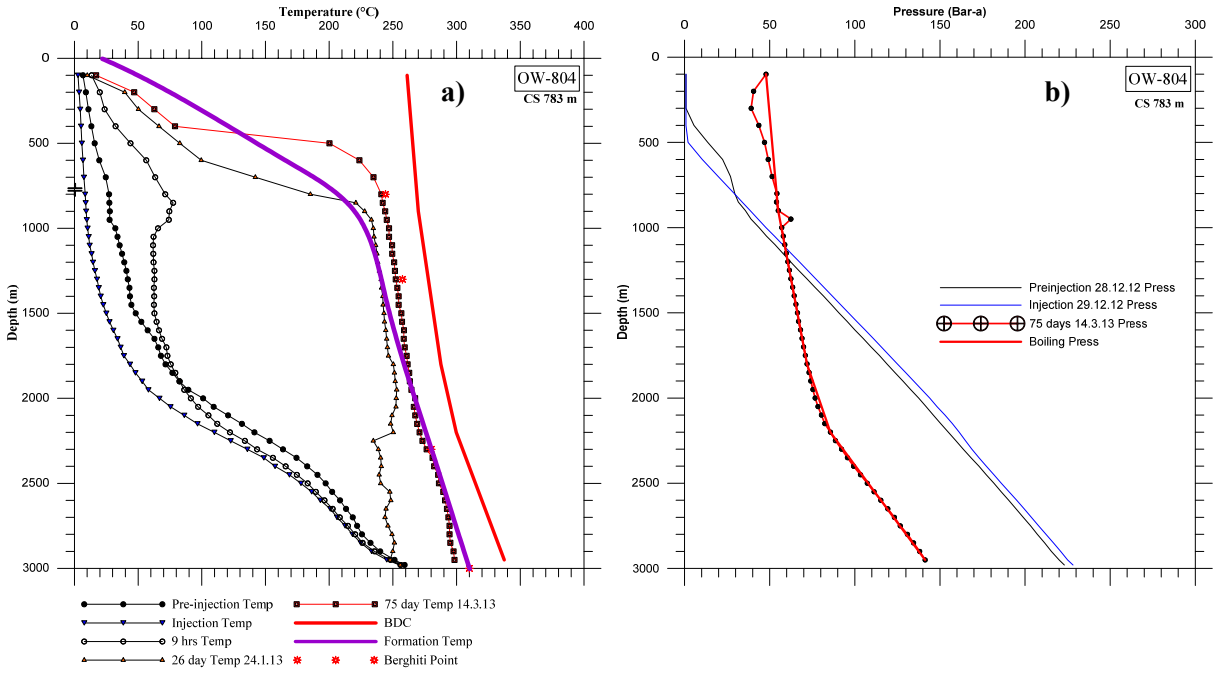

FIGURE 9: Well OW-804: a) Temperature profiles; b) Pressure profiles

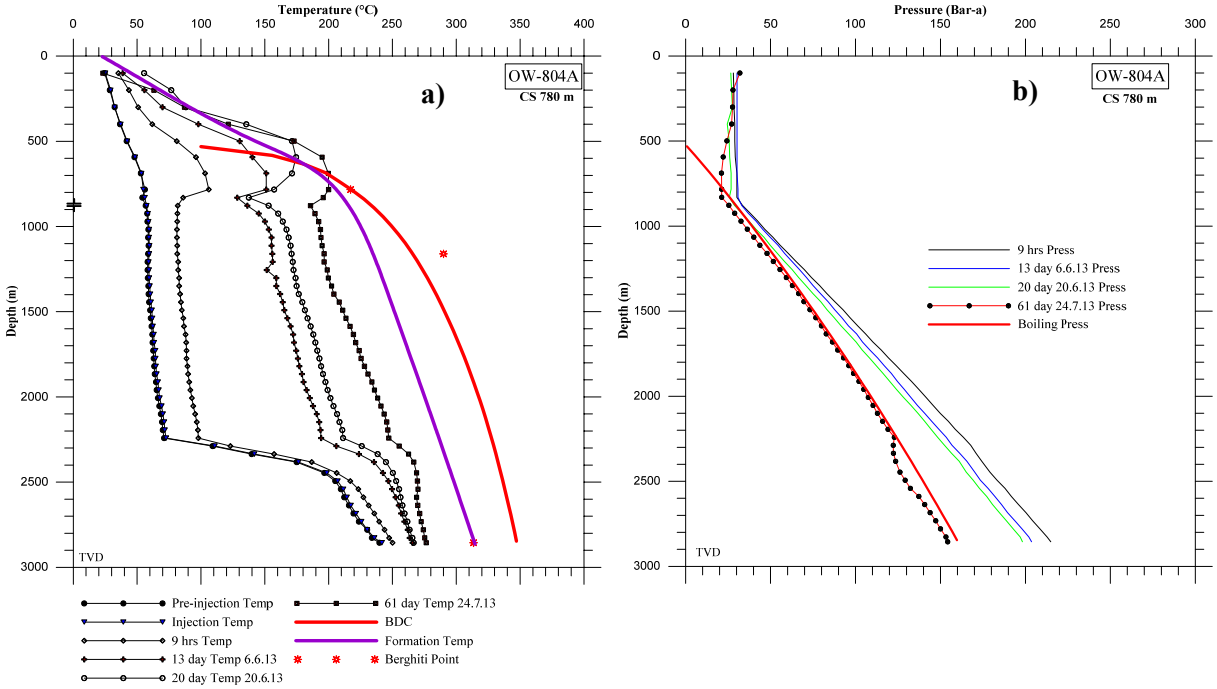

FIGURE 10: Well OW-804A: a) Temperature profiles; b) Pressure profiles

temperatures (BHT). All these temperatures are considered high and are not significantly lower than those encountered elsewhere in Olkaria. However, in the adjacent Olkaria East production field, most wells produce from steam fed reservoirs at shallow depths, and liquid zones at greater depths. This does not seem to be the case in these wells, except for Well OW-802, which bears a resemblance. Deliverability of these wells could be limited by this fact. In some cases, at the Olkaria Domes field, marginal wells with similar profiles as these have turned out to be poor wells. However, wells in this field have appreciably higher permeability that their counterparts in the margins of the Domes field. A

good example is seen in Wells OW-917, OW-918 and OW-918. Pressure situations in Olkaria Southeast wells closely resemble observations elsewhere in Olkaria.

TABLE 1: Summary of well temperature and feed zones

Well name	Type	DepthTVD (m)	Casing shoe TVD (m)	Measured BHT (°C)	Main feed zone TVD (m)	Other feed zone TVD (m)
OW-1	Vertical	1003	418	126	...	...
OW-801	Vertical	2000	847	215	950	1350
OW-801 R1	Vertical	600	190	87	350	300 500
OW-801 R2	Vertical	640	266.7	103	500	350 550
OW-802	Vertical	3000	732.7	280	1050	850 1800 2000 2500
OW-802A	Directional N137°E	2860	785.3	220	1800	850 2500
OW-803	Vertical	3000	861.68	230	1500	1300 1800 2500 2850
OW-804	Vertical	3000	782.65	300	1900	850 1500 2200 2900
OW-804A	Directional N145°E	2870	796.7	280	2250	1200 1300 1450 2450

Physical conditions:

The early wells drilled in the Olkaria Southeast field were shallow and only penetrated into the sharp thermal gradient of the reservoir cap rock. Well OW-801 achieved some convective character at depth but that occurred at non-commercial temperatures. More recent deep drilling has proved the existence of a resource, at least in the northeast margins of the field closest to known structures. The wells presently under study are located near significant structures in the area and are therefore likely to be reasonable producers. Reservoir temperature ranges from 230 to 360°C with the highest located near known structures. Reservoir fluids are likely to be liquid dominated with boiling processes commencing only at the wellbores of Wells OW-802, 802A, 803, and 804A. It is notable, however, that most of these wells have seldom reached stable formation conditions and, therefore, physical conditions may change with more recovery. Figure 11 shows the formation temperatures calculated from available warm up profiles. Some corrections were performed to compensate for the effects of convection in the wellbores and short warm-up periods in a few cases.

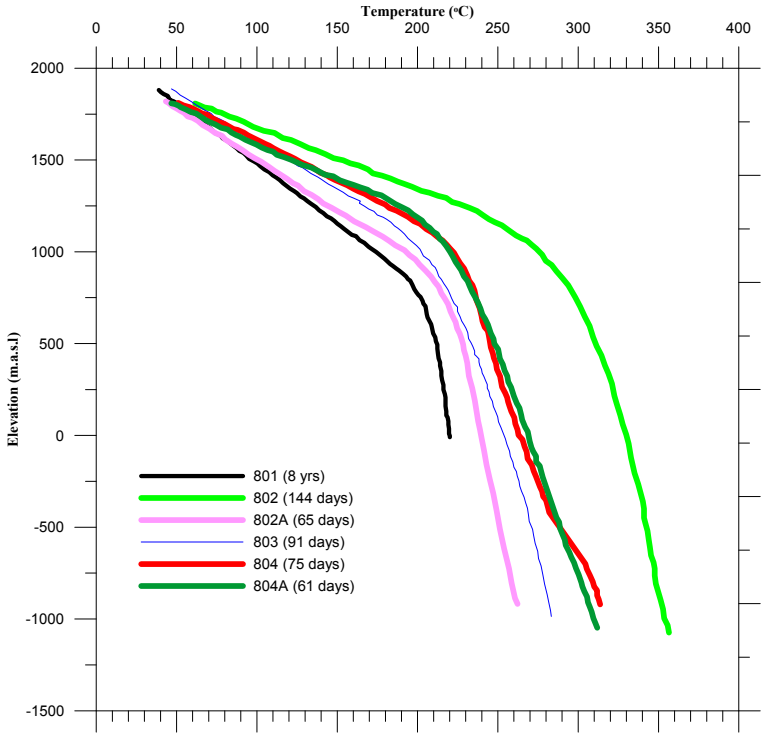

FIGURE 11: Formation temperature profiles

3.1.2 Temperature gradient analysis

It is necessary to characterize the reservoir in this field to find out its probable size, nature, geometry and physical conditions. This is the ultimate goal of the drilling exercise which is currently on-going.

With only limited data available during the course of writing this project, the task can still be accomplished reasonably well. However, data is limited to the south of Ololbutot and covers only a small fraction of the possible resource area. The approach taken here is to collate available information to study the similarities and lack thereof to the adjacent Olkaria East field whose reservoir is well studied. The Olkaria East reservoir is two-phase with a shallow (<1000 m) steam cap formed after more than thirty years of production. Recent wells drilled from the East field under the Ololbutot lava flow proved to be good producers. Such a well is Well OW-11A which delivers two phase fluids in excess of 23 kg/sat discharge enthalpy of 1950 kJ/kg. The main production of the well is located deep in the well and is associated with the North-West trending fault. The same fault controls permeability and fluid movement distribution in the Olkaria Southeast field. Other minor faults trending north-northeast intersect with this fault further south.

The first question addressed here, therefore, is how similar or different is the reservoir at Olkaria Southeast field from those already well known in the greater Olkaria field. To begin with, a filtering analysis is necessary to determine how its temperature relates to some common standard. Axelsson and Gunnlaugsson (2000) arbitrarily defined high-temperature geothermal fields as those reaching temperatures above 200°C at one kilometre depth. Well temperature profiles were filtered by assuming a steep conductive thermal gradient reaching 200°C at 1000 m, which defines a high-temperature system. The convective part of the system was also filtered according to the boiling point curve.

The results show the field is well above the threshold of a high-temperature geothermal field up to a depth of 1000 m. However, the oldest wells in the field, namely Wells OW-1 and OW-801, do not meet this threshold. It appears that the thermal gradient falls quite drastically from Well OW-801 towards Well OW-1 and increases sharply in a North-North-East direction, reaching a peak at Well OW-802.This indicates the existence of a system with the hottest region centred on Well OW-802 and which is deeper than that at the nearby OEPF. It is argued here that perhaps the system could actually be joined at depth, and that two up flows exist, one on either side of the North West-South East fault, passing through the Ololbutot lava flow. The sharp contrast in the temperatures at the conductive depth defines the location of the shallowest up flow to be closest to the wellpads of Wells OW-802 and OW-804. Away from the fault, the system cools as it gets farther away from the hot area in the direction of Well OW-1.

The convective part of the system suggests the reservoir either follows the boiling point curve or a fraction of it. Some of the wells considered here have not fully recovered from drilling and, therefore, may reach temperatures slightly higher than those found in the present study. Well OW-801 is shallowest and has fully heated up, reaching about 80% of the boiling point curve at depths below 1500 m. Well OW-802 has temperatures much higher than the boiling point while its neighbour, Well OW-802A, which was drilled SSE, reaches only 85% of the boiling point. Well OW-803 is currently the most southerly of the new cluster of wells and has temperatures following 90% of boiling point. Both wells in the 804 pad closely approximate the boiling point at about 95%. Well OW-804A was also drilled SSE with a trajectory closer to Well OW-802A and intersects more permeable zones.

The possibility of these wells discharging two phase fluids is, therefore, apparent from these results. This reservoir, however, lacks the traditional shallow steam zone commonly intersected in the neighbouring field. In most wells, moderately hot aquifers are encountered near the casing shoe before reaching the mature convective cell.

It is proposed here that the NW-SE fault passing through Ololbutot lava flow acts as a hydro-geological barrier, separating the fields while providing conduits to sustain a constant pressure boundary.

3.2 Temperature distribution

It is important in the analysis of well temperature profiles not only to study each well individually but also to study the spatial distribution. Temperature distribution in space helps in characterizing the field,

especially in locating up flow and inflow zones. Drill-hole locations are usually targeted in up flow areas. Local temperature distribution also helps to map permeability distribution. It should be noted here that there are few drill holes in the area and they are somewhat stacked together in the northeast margin of the field. The isotherms presented here, therefore, should be looked at with this limitation in mind.

Temperature iso-maps
Horizontal maps of temperature distribution were made at five elevations: 1000, 500, 0, -500 and -750 m a.s.l.

Temperature at 1000 m a.s.l. At this depth, the temperature rises in the eastern half of the field reaching its maximum around Well OW-802 (Figure 12). A shallow colder incursion into the area is observable, trending in a NW fashion, which corresponds roughly to the main structure in the region. Sparse data to the west shows a progressively colder region away from the hotter zone. The 200°C contour reveals a NS trending thermal anomaly with a significant structural barrier passing in between well pads 802 and 804. Well OW-803 is located at the westernmost margin of this anomaly.

*Temperature at 500 m a.s.l.*Temperature is distributed in a similar fashion as that observed at 1000 m a.s.l. with the anomaly now covered by the 230°C contour line (Figure 13).

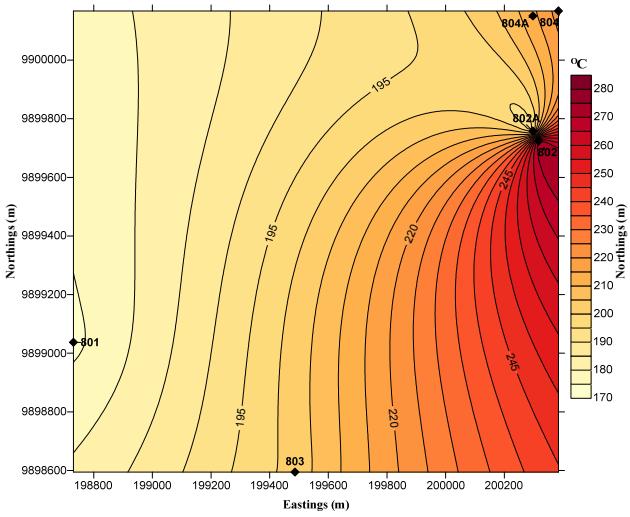

FIGURE 12: Temperature contour map at 1000 m a.s.l.

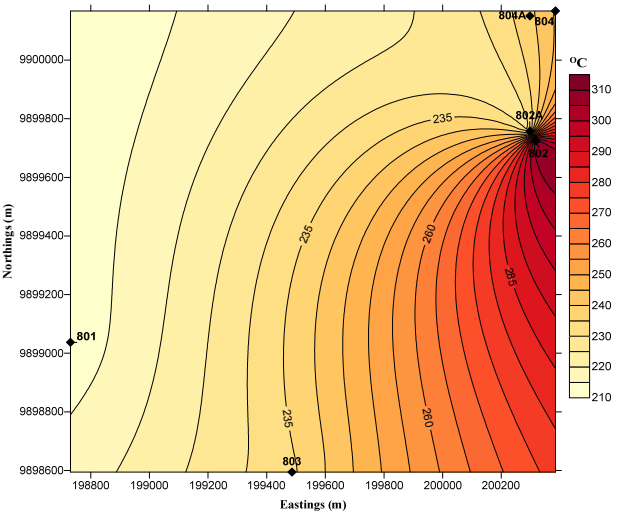

FIGURE 13: Temperature contour map at 500 m a.s.l.

Temperature at 0 m a.s.l. (sea-level). This level corresponds approximately to 2 km depth in this field. Three quarters of the area lies under the 240°C contour line with the same area discussed earlier being under a significantly higher thermal anomaly. The cold incursion attributed to a NW tending structure lessens but its effect is still clear (Figure 14).

Temperature at -500 m a.s.l. Only the newly drilled wells reach these depths. Figure 15 shows that the temperature distribution follows an already observed trend.

Temperature at -750 m a.s.l. At this depth, the thermal anomaly observed earlier is defined by

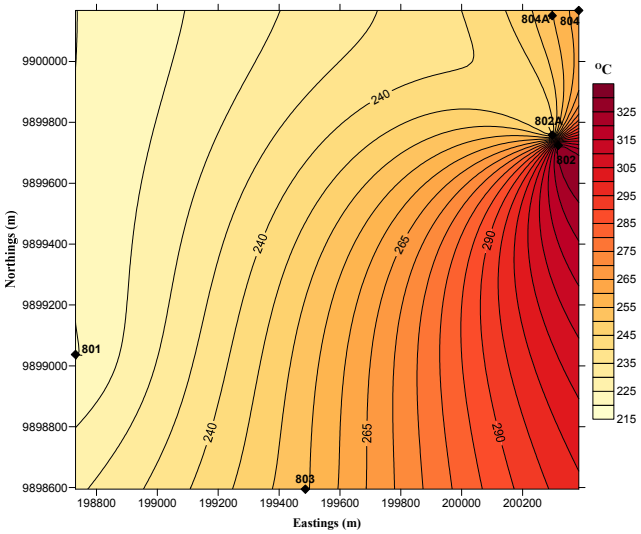

FIGURE 14: Temperature contour map at sea-level

temperature above 275°C. A strong N-S trend is observable here and the incursion of the colder area is more defined in a NW fashion (Figure 16).

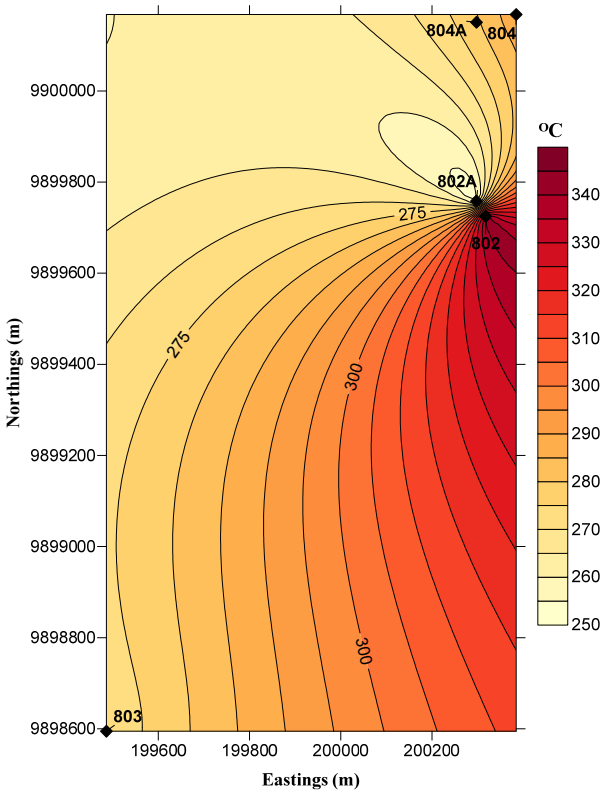

FIGURE 15: Temperature contour map at -500 m a.s.l.

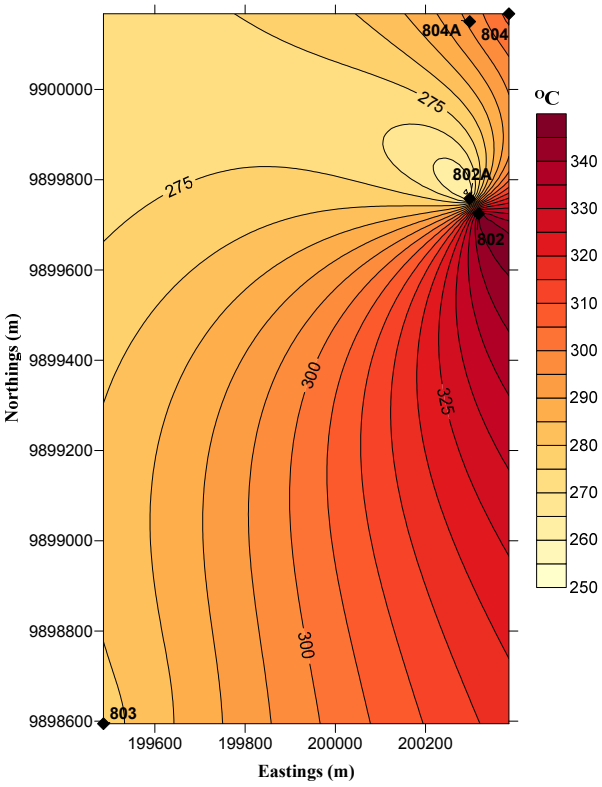

FIGURE 16: Temperature contour map at -750 m a.s.l.

Temperature profiles

Four profiles or cross-sections were taken across the field to study the temperature distribution at depth in selected directions. The first two profiles were taken across the field E-W (Profile 1) and N-S (Profile 2), and the next two were chosen to intersect selected wells in the field: Well OW-1 through OW-804 (Profile 3), and Well OW-803 through Well OW-804 (Profile 4).

Profile 1 shows typical geothermal reservoir temperature behaviour with capping at about 1100 m a.s.l. and the mushroom doming up from great depths into the shallow crust at temperatures above 240°C (Figure 17). The mushroom is strongly vertical and narrow; it is centred between the wellpads of Wells OW-803 and OW-802. It is elongated diagonally, getting deeper to the west. There exists a barrier traversing through the area just east of Well OW-804's pad which strongly suggests a deep fault responsible for a downthrown profile and a temperature reversal in the directional Well OW-804A.

Profile 2. Temperature variations in the N-S profile (Figure 18) suggest the reservoir is centred on Well OW-802 and upwelling of fluids from a deep reservoir is vertically controlled. The hottest region appears not to reach the bottom of Well OW-804A which was drilled directionally to the southeast, suggesting it leaves the centre of the up flow at depth. Temperature decreases to the southern margins of the study area. However, temperature rises considerably to the extreme southerly Well OW-803, showing perhaps good temperatures may exist in that direction. The likely interpretation of this behaviour is that fluid upwelling is strongly controlled by N-S and NNW-SSE trending structures which Well OW-801 does not seem to intersect. Towards Well OW-803, the well intersects a significant permeable zone.

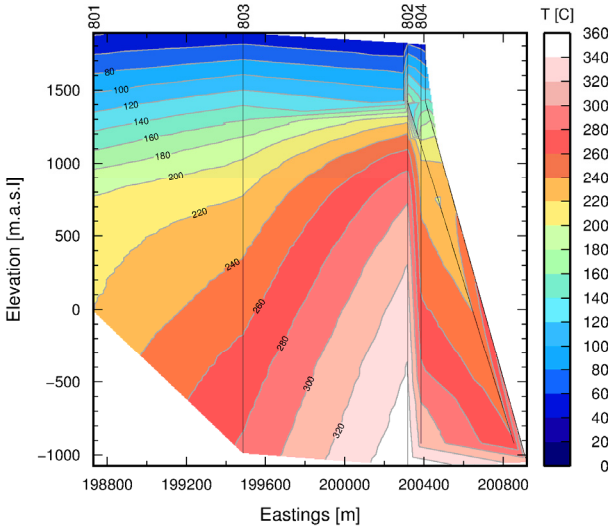

FIGURE 17: Temperature cross-section along profile 1

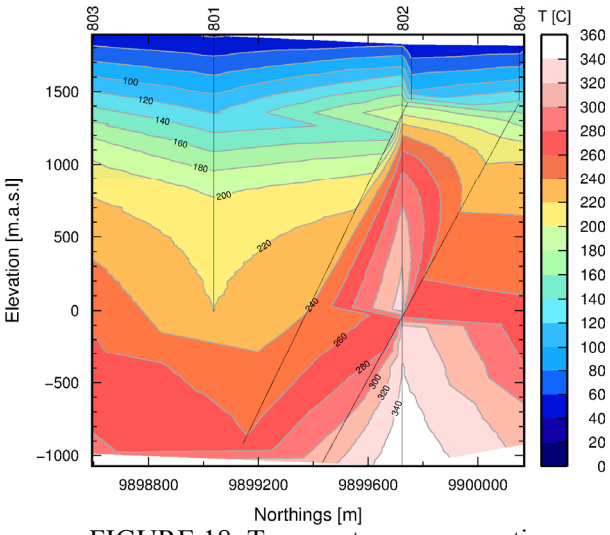

FIGURE 18: Temperature cross-section along profile 2

Profile 3 (Figure 19) is taken from Well OW-1 and elongates in a northeasterly direction, ending at Well OW-804. The profile considers vertical wells falling in between. The temperature distribution along this profile is mushroom shaped, centred at Well OW-802. The reservoir is capped around 1200 m a.s.l. corresponding to about 700 m depth where temperature rises sharply reaching over 300°C, just half a kilometre deeper. The hotter region gradually falls to greater depths towards the start of the profile. It can be generally confirmed here that temperature falls with distance away from Well OW-802 in the direction traversed by profile 3. The existence of a deeper temperature barrier in the opposite direction is observable as well with slight temperature reduction observed in Well OW-804, which corroborates well with the situation in profile 1.

Profile 4 strikes in a north-northeast direction from Well OW-803 and traverses through Well OW-802 and ends at Well OW-804, covering close to two kilometres. The narrow reservoir temperature distribution is clearly conserved here (Figure 20). Considering the 280°C contour, the bottom of the mushroom covers over 2 km and narrows upwardly. The reservoir cap is consistently located at about 700 m depth and is deeper in the regions of Well OW-803, away from the main fault.

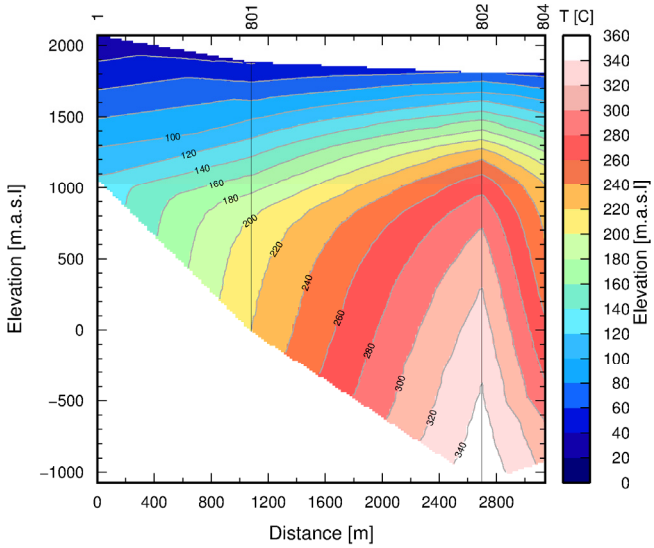

FIGURE 19: Temperature cross-section along profile 3

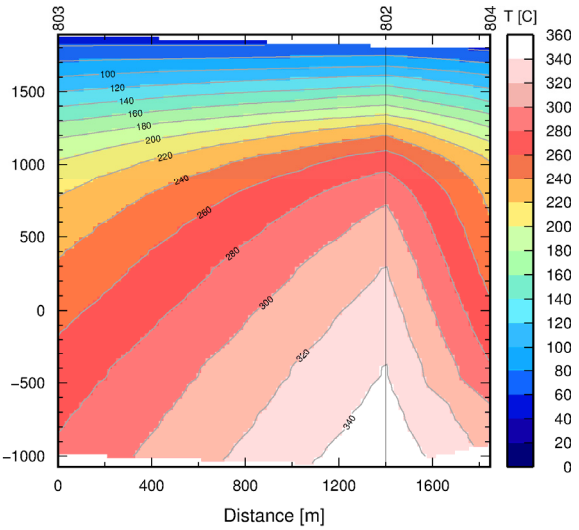

FIGURE 20: Temperature cross-section along profile 4

3.3 Pressure distribution

Evaluation of initial pressure in this field shows all deep drill holes are in a somewhat similar pressure regime. Figure 21 shows the pressure profiles which lie approximately in the same range as in the Olkaria East field. Well OW-802, however, departs slightly at great depths due to the influence of steam in the wellbore as it has heated up the longest. Well OW-802 is also located at the centre of the upflow region. Comparatively, these pressures agree reasonably well with the initial reservoir pressures evaluated during injection testing and which are reported in the next chapter.

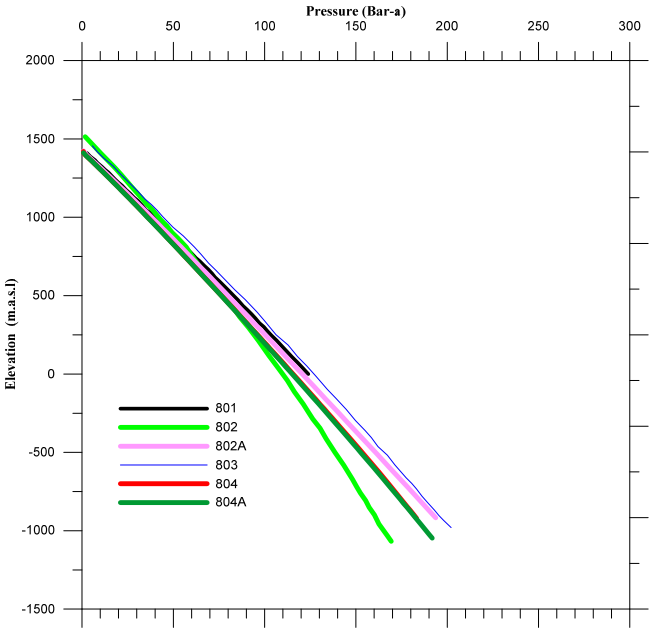

FIGURE 21: Initial pressure profiles

Pressure iso-maps
Pressure gradients are the driving force of geothermal fluids up the wellbore. It is very common for high pressure wells to deliver more at the wellhead. Pressure potentials drive fluids between aquifers. Understanding pressure distribution in space is, therefore, very important in deducing the flow directions of geothermal fluids. Similar depths investigated for temperature in Section 3.2 were also studied to understand the spatial pressure behaviour in the field. It should also be noted here that at present only a few drill holes have been drilled in the area and their locations are stacked in the northeast margin of the field.

Pressure at 1000 m a.s.l. High-pressure regimes are located in the southeast margin of the study area and a northwest trend was deduced for possible fluid movement at this depth (Figure 22). Of importance to note is the most pressurized region is located around Well OW-803. The high-pressure regime then eases outwardly in the direction of Well OW-801 and northwards.

Pressure at 500 m a.s.l. The highest pressure regime is localized at Well OW-803 and eases outwardly in all directions (Figure 23). At this depth, which corresponds to depths in excess of 1400 m, pressures in the region of 80 bar-a are prevalent. Likely fluid movements at this depth are, therefore, deduced to be in a northeast direction.

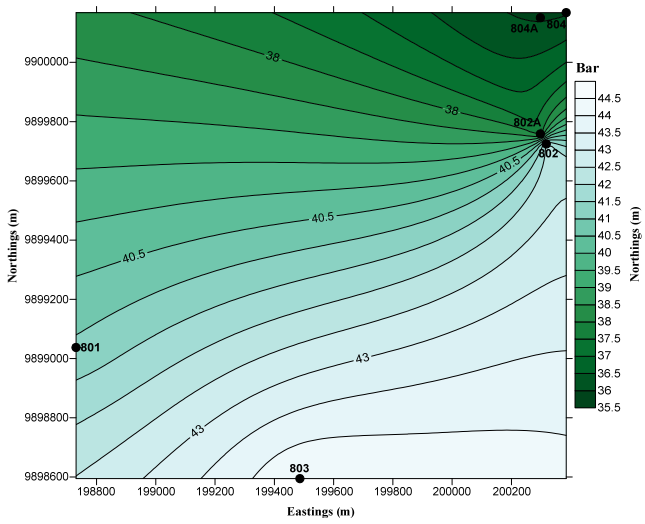

FIGURE 22: Pressure contour map at 1000 m a.s.l.

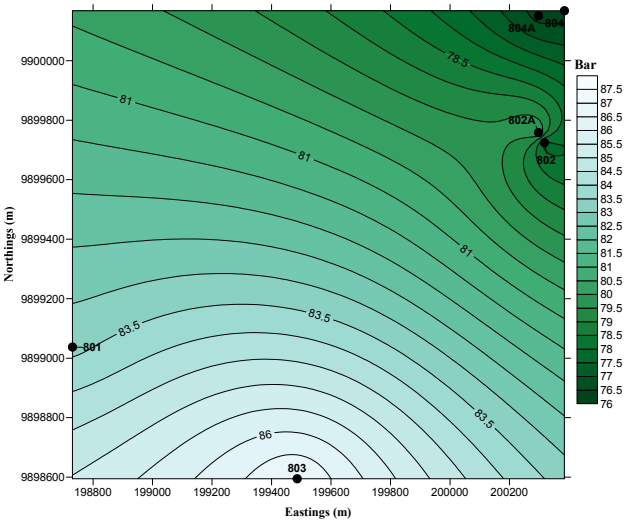

FIGURE 23: Pressure contour map at 500 m a.s.l.

Pressure at 0 m a.s.l. *(sea-level).* A significant pressure gradient exists between the two non-artesian wells located in the southern and southwest parts of the field and their counterparts to the northeast (Figure 24).

Pressure at -500 m a.s.l. At this depth, a strongly NW-SE trending high-pressure region is evident in the vicinity of the wells on the 802 well pad (Figure 25). The highest pressure observed in Well OW-803 persists at this depth.

Pressure at -750 m a.s.l. A similar situation persists as already observed at -500 m a.s.l. with increasing pressure gradient observable (Figure 26). Fluid flow directions at well bottoms are particularly directed toward Well OW-802, interpreted as the centre of the upflow area.

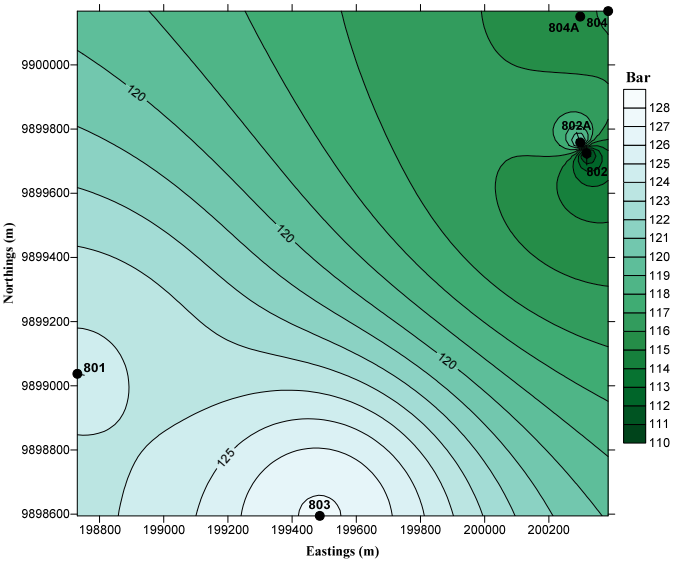

FIGURE 24: Pressure contour map at sea-level

Pressure profiles

The same profiles or cross-sections considered for the temperature distribution (Section 3.2) were also considered for a pressure analysis.

Profile 1. Pressure distribution along this profile shows doming of a high-pressure region, peaking at Wells OW-802 and OW-804 and elongating to the west. The western part show uniform distribution between Wells OW-801 and OW-803, suggesting a boundary of the high-pressure regime. The highest pressure region at depth is located just at the bottom of both wells drilled on the 804 pads and 802 pads (Figure 27).

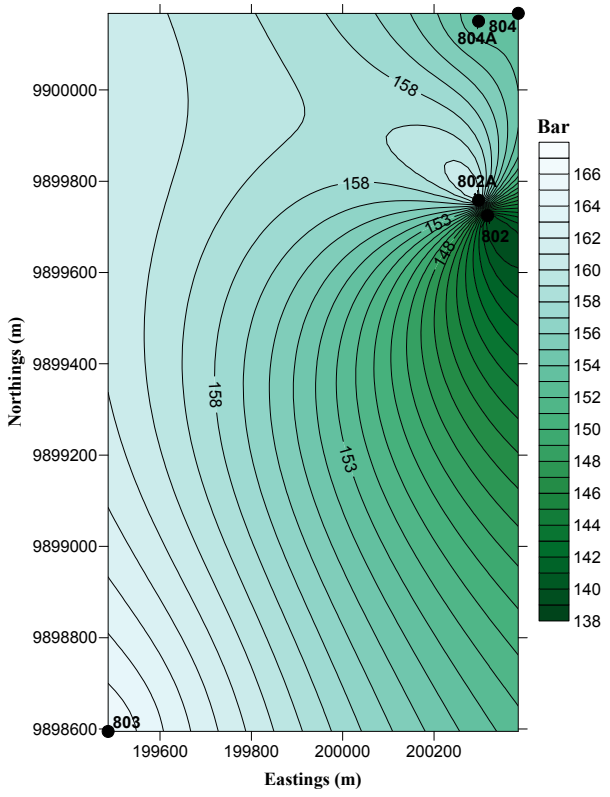

FIGURE 25: Pressure contour map at -500 m a.s.l.

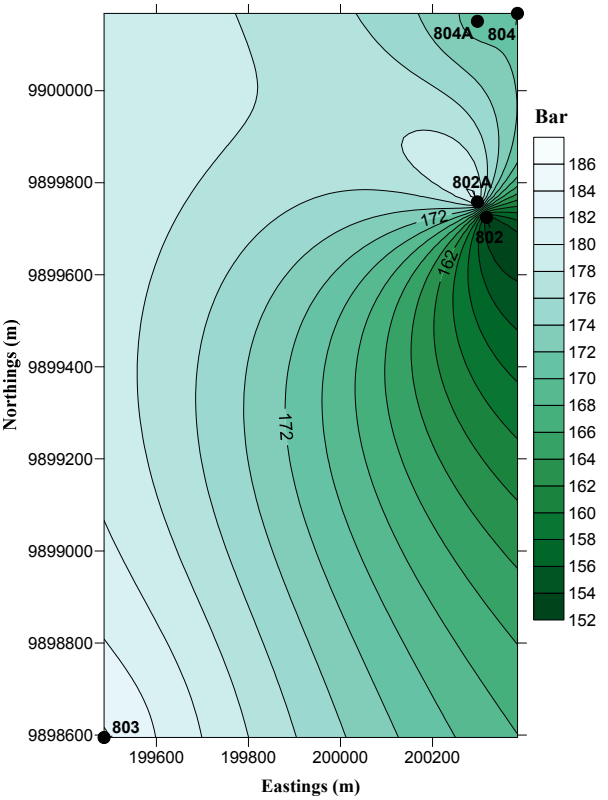

FIGURE 26: Pressure contour map at -750 m a.s.l.

Profile 2. High pressure regimes exist in the northernmost margins of the field and stretch to the central part of the field before decreasing almost drastically as you move away from the structures near Ololbutot lava flow (Figure 28). This structure suggests a down flow associated with the margins of the mushroom shaped structure of the temperature profile. Hot water rises at the centre of the mushroom centred near Well OW-802 and flows away to great depths to the west and southwest of the area. The up doming of fluids in Well OW-803, already seen in temperature profile 2, is attributable to an intersection of another permeable structure.

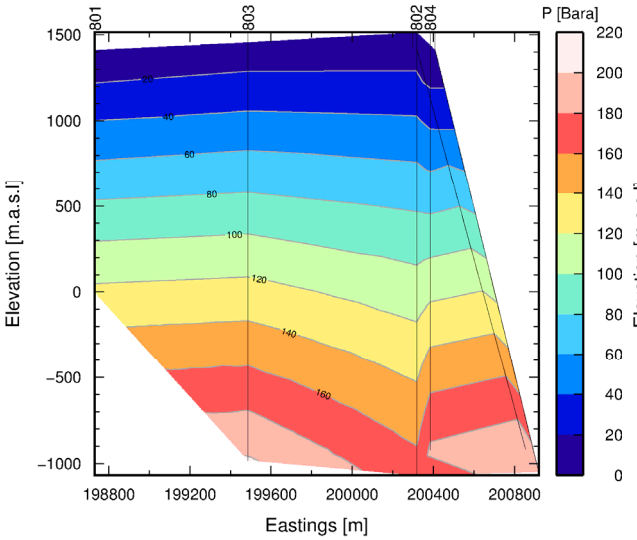

FIGURE 27: Pressure cross-section along profile 1

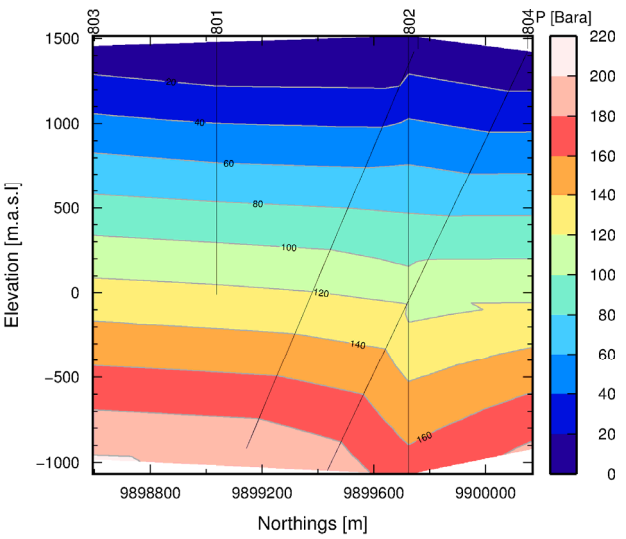

FIGURE 28: Pressure cross-section along profile 2

Profile 3 (Figure 29) is limited by the absence of measured pressure at Well OW-1 and, therefore, shows a similar distribution as that of temperature only beginning at Well OW-801. A similar trend is observed where high-pressure regimes fall towards the end of the profile and decline in pressure towards the opposite side.

Profile 4. The pressure distribution is consistent with all other profiles rising towards the fault and diminishing in the opposite direction quite drastically (Figure 30). The main production in Well OW-803 is actually deeper where the most permeability exists and at locations where higher pressures are intersected in the region. This attribute is typical for the marginal areas of the mushroom temperature behaviour in geothermal reservoirs.

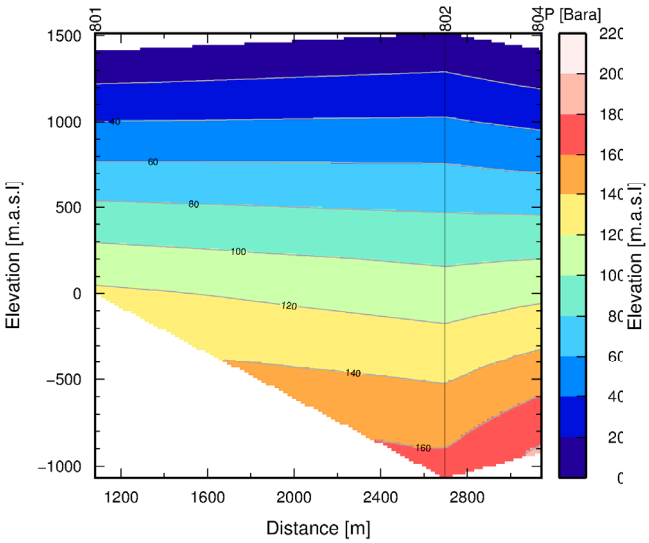

FIGURE 29: Pressure cross-section along profile 3

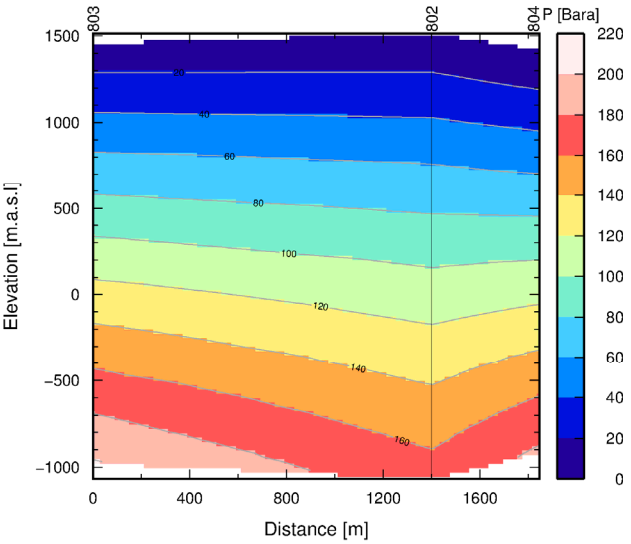

FIGURE 30: Pressure cross-section along profile 4

3.4 Alteration mineralogy

Composition of geothermal fluids is controlled by temperature dependent reactions between the rock and fluid. The resulting hydrothermal alteration products are affected by temperature, pressure, rock type (at low temperatures), permeability, fluid composition and duration (Brown, 1978). These minerals provide a historical evolution of temperatures in the system.

Particular alteration minerals have been employed in different fields as a kind of geothermometer. While this is mainly field dependent, the Olkaria experience (Omenda, 1998) with mineral formation temperature does not differ largely with those observed elsewhere, e.g. Reyes (2000), and are, therefore, adopted here.

In this study, two minerals were chosen for this purpose. The first appearance of epidote maps formation temperatures of 240°C being encountered, and that of actinolite-biotite gives temperatures in excess of 280°C. The first appearances of these minerals were plotted alongside established temperature profiles in the field. Figure 31 shows reasonable correlation between the two thermometers to the east of the field, and a departure in the colder part of the field, mainly in Wells OW-801 and OW-803. In this section of the study area, temperatures shown by mineralogy are much lower than the actual measurements in drill holes. This is a consequence of cooling further away from the established upflow and known fluid conduits in the area.

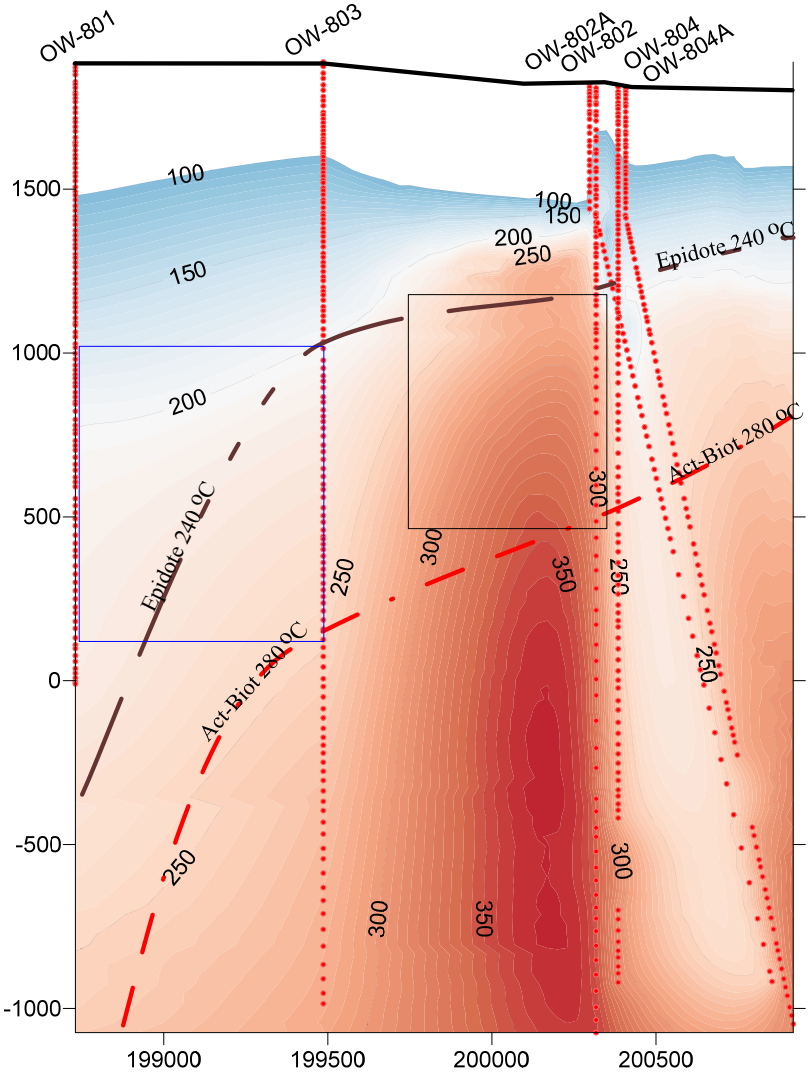

FIGURE 31: Relationship between formation temperature and alteration mineralogy at OSEPF; Black dotted line shows first appearance of epidote; red dotted line shows first appearance depths of actinolite or biotite; blue rectangle shows regions of cooling; black one shows regions of either equilibrium or heating

3.5 Well simulation

3.5.1 Theory

The flow of geothermal fluid flowing vertically in a well can be expressed by using two sets of mathematical equations. Between the feed zones, the flow is represented by one dimensional steady state equations of momentum, energy and mass flux equations. In the case of a feed zone being encountered, mass and energy balances are then required between the fluid already in the wellbore and the incoming fluid. By applying boundary and initial conditions that fully describe the problem, the

governing equations can then be solved numerically. The solutions to these equations involve taking small finite sections of the pipe from the origin of the fluid to the top, thus a continuum from the feed zone to the wellhead is solved. It is also possible to solve the equations from top to bottom, as well, with an appropriate description of the flow.

The governing steady-state equations for mass, momentum and energy flux for a vertical flowing well is set up in Equations 3, 4, and 5.

$$\frac{d\dot{m}}{dz} = 0 \tag{3}$$

$$\frac{dP}{dz} - \{\left[\frac{dP}{dz}\right]\text{fric} + \left[\frac{dP}{dz}\right]\text{acc} + \left[\frac{dP}{dz}\right]\text{pot}\} = 0 \tag{4}$$

$$\frac{dE}{dz} \pm Q = 0 \tag{5}$$

where $\dot{m}$ = Total mass flow;
z = Depth:
P = Pressure;
E = Total energy flux;
Q = Ambient heat loss over unit distance.

In case a feed zone is encountered, flow between the well and the reservoir gives the governing equation of the form:

$$\dot{m}_{feedzone} = PI\left[\frac{k_{rl}\rho_1}{\mu_l} + \frac{k_{rs}\rho_{rs}}{\mu_s}\right](P_r - P_l) \tag{6}$$

where $\dot{m}$ = Flow rate from feed zone;
PI = Productivity index of feed zone;
k_{rl} = Relative permeability in liquid phase;
k_{rs} = Relative permeability in steam;
ρ_l = Density of liquid;
ρ_{rs} = Density;
μ_l = Dynamic viscosity of liquid;
μ_s = Dynamic viscosity of steam;
P_r =Reservoir pressure;
P_l =Well pressure.

The HOLA well simulator presented by Björnsson (1987) solves these equations for vertical wells from the bottom feed zone up the well. The bottommost feed zone need be at the bottom of the well and the flow into the well is defined as positive; the flow from the well outwardly into the formation takes the negative sign. Different computation modes are available in HOLA for simulations with different known parameters.

In this work, computation mode 2 was applied for predicting the output curves, given known relative feed zone flow rates and calculated enthalpy conditions. The Orkiszewski velocity model (Orkiszewski, 1967) was assumed to describe the phase velocity in the wells.

3.5.2 Results

The program HOLA was used to estimate the productivity curve for candidate wells in OSEPF. The thermodynamic parameters used were calculated from observed pressure and temperature conditions during warm up, discussed in Section 3.1. The well productivity indices were estimated by taking the assumption that it equals a third of the well's injectivity indices (Grant and Bixley, 2011) and relative contributions assigned to the feed zones in the well.

Results show liquid wells producing at low pressure regimes with moderate deliverability (Figure 32).

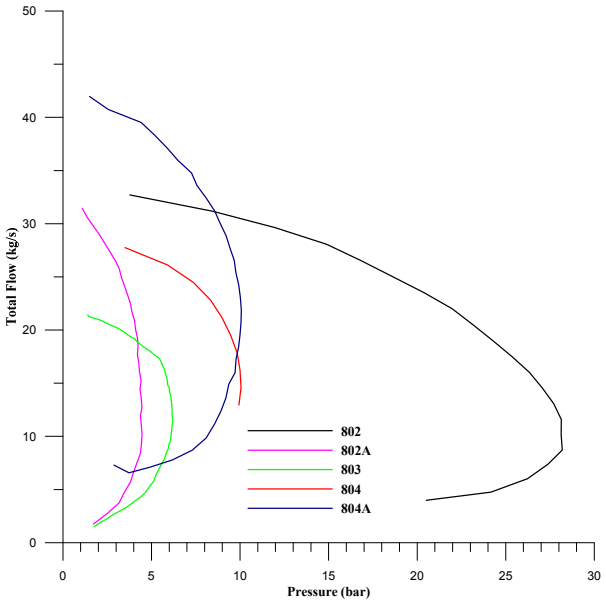

FIGURE 32: Calculated output curves

4. PRESSURE TRANSIENT ANALYSIS

4.1 Theoretical background

The basis of pressure transient analysis lies in the partial differential equations describing single phase flow in porous media. However, we are concerned with only a limited part of the problem involving describing pressure responses in the reservoir as measured in the vicinity of a well penetrating into the reservoir. In geothermal situations, fractures play a more important role in controlling reservoir permeability than porous rock. Darcy's law is used to describe fluid flow in a porous media. The resulting equation can be extrapolated to fractured media since, on a large scale, such as the case of geothermal reservoirs, fractures behave as porous rock. We expect to see immediate wellbore effects and gradually transit to boundary effects at later times in a well test. The pressure diffusion equation (Equation 7) describes the flow within the infinite acting reservoir with appropriate boundary conditions applied to describe flow in the outer margins. The pressure diffusion equation takes the form of a heat diffusion equation in all respects. The two processes are, therefore, comparable.

$$S\frac{\partial p}{\partial t} = \frac{k}{\upsilon}\nabla^2 p - f(x,y,z) \tag{7}$$

where S = Storativity;
p = Pressure;
t = Time;
k = Permeability;
υ = Kinematic viscosity of water;
$f(x,y,z)$ = Mass source density.

4.2 Description of injection tests at Olkaria

Pressure response is measured by injecting cold water at varying rates at the top of a well soon after the well is completed and cased. The availability of the rig on site is important as they often have good pumping capability and reliable water supply. There are cases where warm brine is used to supplement cold water. The two waters are mixed together in collection tanks so that no significant thermal contribution from injected water is envisaged.

A typical well completion test program involves taking temperature and pressure profiles in the beginning as soon as the slotted liner is lowered into the well. This profile is mainly used to locate appropriate permeable zones from where to monitor pressure response during injection. The location of such points is chosen depending on permeability contrast between different feed zones and pressure tolerance of the measuring tool for the length of pressure monitoring. The measuring tool is then lowered to the chosen depth and step rate injection begins. Typically, there are three injection steps of 5 l/s, from 16.67, to 31.67 l/s, each lasting for three hours. The initial injection at 16.67l/s is usually four hours long and seldom has any observable effects on reservoir pressure. After three hours of injection at the greatest pumping rate (31.67 l/s), another temperature and pressure profile is taken without stopping the injection. There is, therefore, a significant gap between this last injection step and the next step where continuous pressure monitoring at the selected depth is discontinued.

Following a successful step rate test, an eight hour long monitoring of pressure draw-down is measured at the same depth where injection response was monitored. This last step is done without any injection into the well at all. This usually gives reasonable pressure draw-down curves despite the drastic pressure fall at the beginning when the pumps are switched off. This is arguably unimportant as more often wellbore storage effects dominate the well and the transition to the infinite acting reservoir response happens at least an hour into the test. By neglecting the apparent sudden drop at the beginning, this paper shows the reservoir and its boundary effects can be successfully modelled.

4.3 Reservoir properties

In this section, common parameters associated with well test analysis are discussed and their relationships with common hydrological parameters of interest in characterizing geothermal reservoir are deduced. The aim of the analysis in a well test is to deduce hydrological parameters that characterize the reservoir penetrated by the well. These parameters are then interpreted to build a hydrological picture of the larger reservoir under study.

Parameters
The *estimated reservoir pressure (P_{est})* and *estimated reservoir temperature (T_{est})* are average estimates for the part of the reservoir that is being investigated in the well test. These values are used to calculate approximate values of the dynamic viscosity of the reservoir fluid and the total compressibility of the rock matrix and the fluid.

Wellbore radius (r_w) is the average radius of the well at the reservoir depth, given in meters.

Dynamic viscosity of the reservoir fluid (μ) is the estimated average viscosity of the fluid at reservoir conditions. In cases where the fluid is in two phases, the average viscosity can be taken as the harmonic average of the two phases, weighted by the mass fraction of each phase, i.e. $\mu_t = (x_w/\mu_w + x_s/\mu_s)^{-1}$, where x_w is the mass fraction of water and x_s is the mass fraction of steam (Horne, 2006).

Total compressibility (c_t) describes the ability of the fluid and reservoir rock to compress or expand as a function of pressure. Formulations for computing compressibility will be slightly different depending on the physics of the fluid and the reservoir, but a further discussion on that can be found in Grant et.al. (1982). Total compressibility will typically be on the order of 10^{-9} Pa^{-1} for a liquid-dominated reservoir, 10^{-7} Pa^{-1} for a dry-steam reservoir, and 10^{-6} Pa^{-1} for a two-phase steam-water reservoir.

Porosity (ϕ) is the volume fraction of the rock which is capable of holding water.

Transmissivity (T), based on volumetric flow, has the SI unit [m^3/Pas]. It describes the ability of the reservoir to transmit fluid, hence largely affects the pressure gradient between the well and the reservoir. Its physical formulation is (kh/μ), where k is the effective permeability of the reservoir, h is the reservoir thickness, and μ is the dynamic viscosity of the active reservoir fluid. The transmissivity can

vary by a few orders of magnitude but common values from injection testing in geothermal reservoirs are on the order of 10^{-8}[m^3/Pas].

Storativity (S) has the SI unit [m^3/Pa m^2 or m/Pa] and defines the volume of fluid stored in the reservoir, per unit area, per unit increase in pressure. Hence, it has great impact on how fast the pressure wave can travel within the reservoir. The general formulation of storativity is $S = c_t h$, where c_t is the total compressibility of the rock and the reservoir fluid, and h is the reservoir thickness. Storativity varies greatly between reservoir types (i.e. liquid-dominated vs. two-phase or dry-steam) because of its dependence on fluid compressibility (Grant et al., 1982).

Skin factor (s) is a variable used to quantify the permeability of the volume immediately surrounding the well. This volume is often affected by drilling operations, being either damaged (e.g. because of drill cuttings clogging the fractures) or stimulated (e.g. due to extensive fracturing around the well). For damaged wells the skin factor is positive, and for stimulated wells it is negative. The typical skin factor in geothermal wells is considered to be in the range -5 - 5, although values may range from about –5 - 20. The skin factor can also be described in terms of the effective wellbore radius, i.e. the apparent radius of the wellbore caused by the skin effect. The effective radius is given by $r_{eff} = r_w e^{-s}$ where r_w is the measured wellbore radius (Horne, 1995). It should be noted that the skin factor and storativity are quite strongly correlated in most well test models, hence the relative accuracy of each parameter will be lowered when both are included.

Wellbore storage (C) is a property that accounts for the difference between the wellhead flow rate, and the "sand face" flow rate (i.e. the flow into or out of the actual formation). Wellbore storage effects can occur in several ways, but most commonly by changing the liquid level and fluid expansion. In injection testing, the most dominant cause for wellbore storage is changing liquid level. The storage effect is caused by the volume in the wellbore itself being emptied or filled. In the case of fluid expansion, consider a drawdown test. When the well is first opened to flow, the pressure in the wellbore drops and the fluid in the wellbore expands, providing the initial production volume (Horne, 1995). Typically under single phase liquid conditions, the wellbore storage, because of fluid expansion, is negligible. However, in a geothermal well where the wellbore fluid changes from a single phase liquid to a two-phase steam-water, the expansion effect can be very significant.

Radius of investigation (r_e) is the approximate distance at which the pressure response from the well becomes undetectable. Hence, this radius defines the area around the well being investigated, although the value of the parameter should be viewed more qualitatively. When boundary conditions are seen in the data, the approximate distance to the boundary will define the radius of investigation.

The *injectivity index (II)* is often used as a rough estimate of the connectivity of the well to the surrounding reservoir. Here it is given in the units [(l/s)/bar] and it is defined as the change in the injection flow rate divided by the change in the stabilized reservoir pressure (Equation 8).

$$II=|\Delta Q/\Delta P| \tag{8}$$

Here $\Delta Q = Q_f - Q_i$ and $\Delta P = P_f - P_i$ where *i* refers to the initial value and *f* refers to the final value. In Well Tester software (Júlíusson et al., 2007), the pressure values used to calculate *II* are taken from the modelled response, not the actual data collected.

Deduced parameters

Two specific parameters of interest in reservoir physics can be deduced by combining the initial parameter estimates and the well test results. The parameters estimated in the well test are the transmissivity (T) and storativity (S) and, given the porosity (ϕ), total compressibility (c_t) and dynamic viscosity (μ), one can estimate the reservoir thickness and the effective permeability from Equation 9.

$$h = \frac{S}{\varphi c_t} \qquad \text{and} \qquad k = \frac{T\mu}{h} \tag{9}$$

However, it should be noted that the error in these estimates is influenced by the combined error in the underlying parameters so, as a general rule, the results should only be viewed as a qualitative cross check on the well test results.

The *effective permeability (k)* is a measure of the ability of the reservoir rock to transmit fluid. Permeability has the SI units $[m^2]$ but is commonly referred to using Darcy units, i.e. 1 D ≈ 10^{-12} m^2. Permeability in geothermal reservoirs is generally on the order of 1 to 100 mD (milliDarcy), i.e. 10^{-15} – 10^{-13} m^2.

Reservoir thickness (h) is the estimated thickness of the formation that is actively exchanging fluid with the wellbore.

4.4 Results of step rate injection tests at Olkaria South East Field

Step-rate injection tests are carried out in all newly drilled wells. Pressure transient data were collected for different injection rates and analyses using Well Tester software. The results of these analyses are tabulated in Table 2. In general, the injection tests were considered successful despite there being few pressure recordings, a common limitation of mechanical tools. Pressure response of data is important in diagnostic exercises to deduce the nature of reservoirs, their sizes and existing boundary conditions. For simplicity, deep reservoirs were considered to be at an average of 240°C with a pressure range of 160-180 bar-a. The area actively exchanging reservoir fluids can be difficult to determine. An estimate of an average 500 m was considered reasonable for the purpose of this study. However, shallower wells had different reservoir thicknesses and expected temperatures.

In the analysis of the injection tests, two kinds of models were considered for the reservoir, on one hand a homogeneous reservoir and on the other hand a dual porosity reservoir. Three different boundary conditions were used in the modelling: an infinite reservoir, a reservoir with constant pressure at the boundary, and finally a no-flow boundary in which case the fluid cannot flow freely across the boundary; but, in that case, the pressure continues to increase with time when the injection rate is kept steady. Best results from the tests showed that the reservoir conforms to the homogeneous reservoir with a constant pressure boundary, and a constant skin with wellbore storage.

TABLE 2: Well test analysis

Well Name	Depth TVD (m)	Main Feedzone TVD (m)	II(all steps) (l/sbar)	Best step	Transmis-sivity×10^{-8} m^3/(Pa·s)	Storativity ×10^{-8} m^3/(Pam^2)	Skin factor	Well bore storage × 10^{-4} m^3/Pa	II (best step) (l/s bar)
OW-801 R1	600	350	4.75	4	3.06	1.14	-6.14	1.12	12.23
OW-801 R2	640	500	4.27	4	2.66	1.41	0.76	1.4	3.47
OW-802	3000	1050	6.95	1	0.74	6.65	-5	0.72	5.34
OW-802A	2860	1800	3.34	3	1.75	6.65	-1.87	0.47	2.92
OW-803	3000	1500	1.12	5	0.84	6.95	-3.15	0.59	1.75
OW-804	3000	1900	4.87	4	3.23	6.75	-2.08	5.55	7.51
OW-804A	2870	2250	4.28	4	6.3	6.75	0.41	5.56	7.23

Well OW-801R1 was modelled with homogenous-infinite-constant-skin with wellbore storage for a 200 m thick reservoir. The injection steps fitted the reservoir model fairly well. Step 4 was considered the best fitted step (Figure 33) which gives injectivity of 12.23 l/s bar and effective permeability of 4.61 x 10^{-14} m^2. Estimates of the injectivity index were, however, lowered when all steps were considered.

Well OW-801R2 was modelled with similar model parameters as Well OW-801R1, and with step 4 returning the best results with an injectivity index of 3.47 l/s bar and effective permeability of 4.75 x 10^{-14} m^2. Figure 34 shows the fit for Step 4.

Well OW-802. Four injection steps were studied for this well. The first step with a homogeneous, constant pressure and wellbore storage with constant skin, fitted well (Figure 35). An injectivity index of 5.34 l/s bar and effective permeability of 1.70 x 10^{-15} m^2 were obtained for this step.

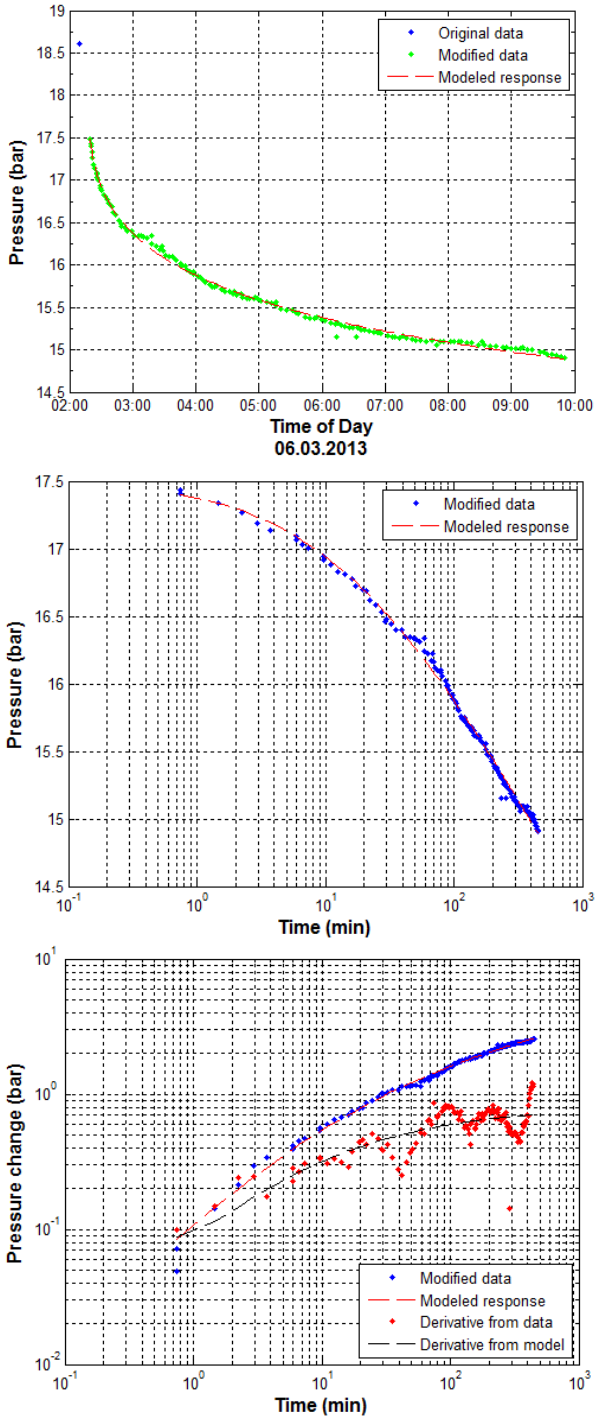

FIGURE 33: Fit between model and collected data in linear, semi-log and log-log scale for step number 4 for Well OW-801R1

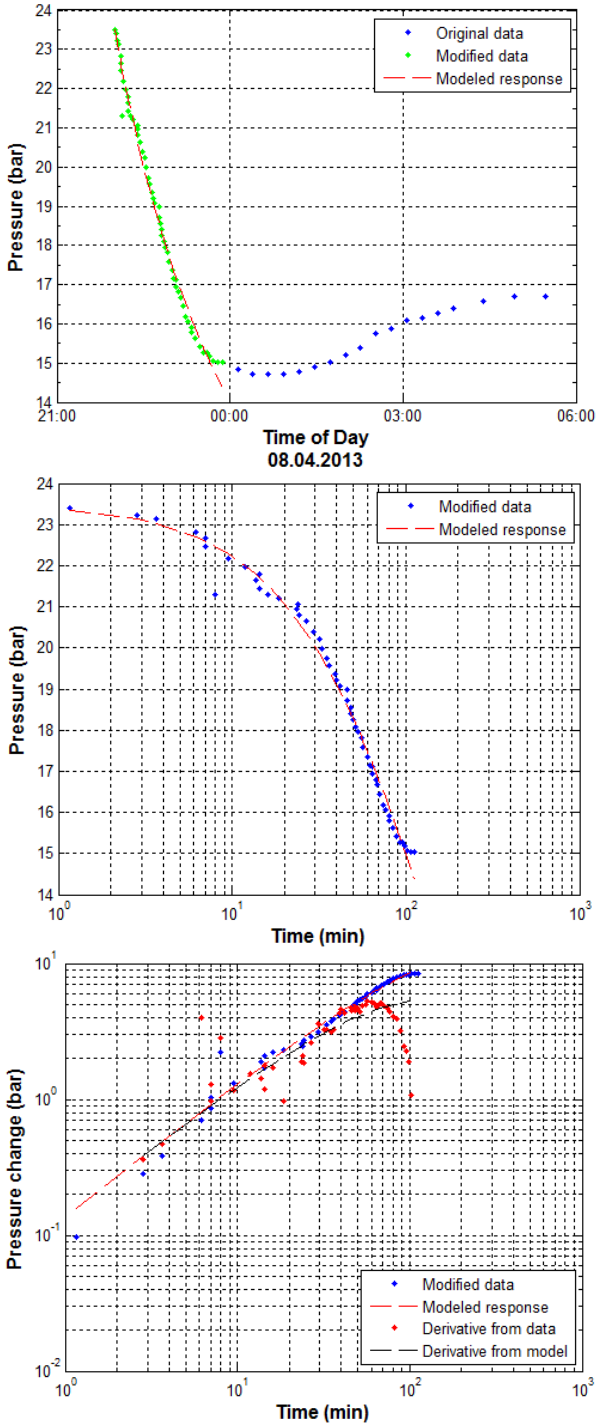

FIGURE 34: Fit between model and collected data in linear, semi-log and log-log scale for step number 4 for Well OW-801R2

Well OW-802A. Three injection steps were considered for this well for a constant pressure bounded homogeneous reservoir with wellbore storage and constant skin. Of the three steps considered, the third step obtained the best fit to the model (Figure 36) with an injectivity index of 2.92 l/s bar and effective permeability of 1.99 x 10^{-15} m^2.

Well OW-803. Five steps were considered in this well. The first and last steps were successfully modelled with homogeneous, constant pressure and constant skin with wellbore storage reservoir model. In a few steps, the reservoir tended to demonstrate no flow boundaries. However, the dominant

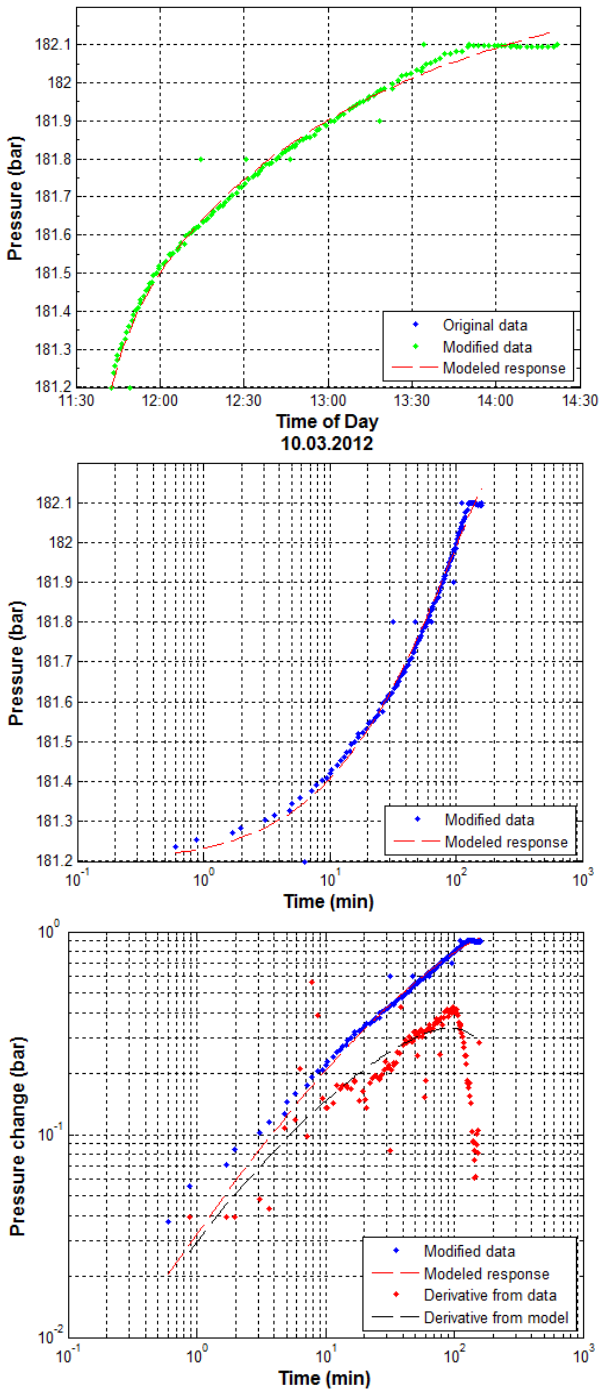

FIGURE 35: Fit between model and collected data in linear, semi-log and log-log scale for step number 1 for Well OW-802

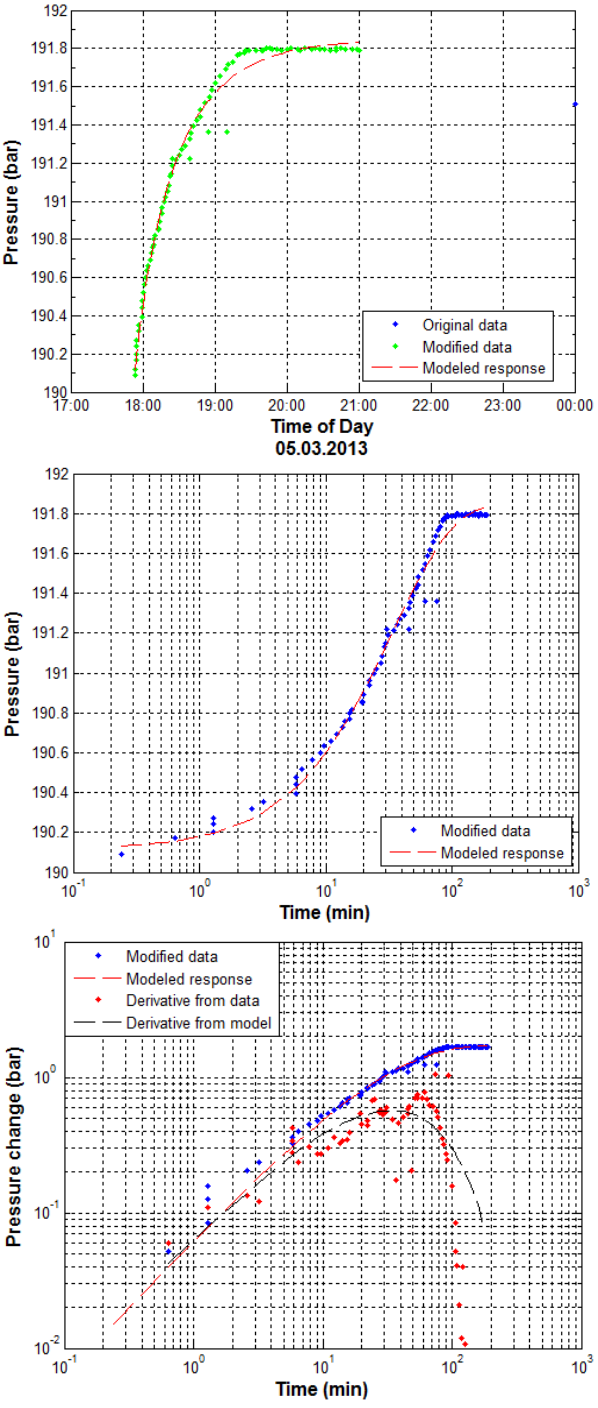

FIGURE 36: Fit between model and collected data in linear, semi-log and log-log scale for step number 3 for Well OW-802A

behaviour was constant pressure with the probable effect of low permeability. The fit in the last step was exceptionally good and returned a low injectivity index of 1.75 l/s bar and effective permeability of 1.74 x 10^{-15} m^2. Figure 37 shows the fit obtained for step 5.

Well OW-804. Four injection steps were modelled as homogeneous, constant pressure and constant skin with wellbore storage reservoir, with step 4 considered the best step based on its fit. Figure 38 shows the linear, semi-logarithmic and logarithmic plots obtained for pressure transient analysis for step 4. The step obtained an injectivity index of 7.51 l/s bar and effective permeability of 7.37 x 10^{-15} m^2.

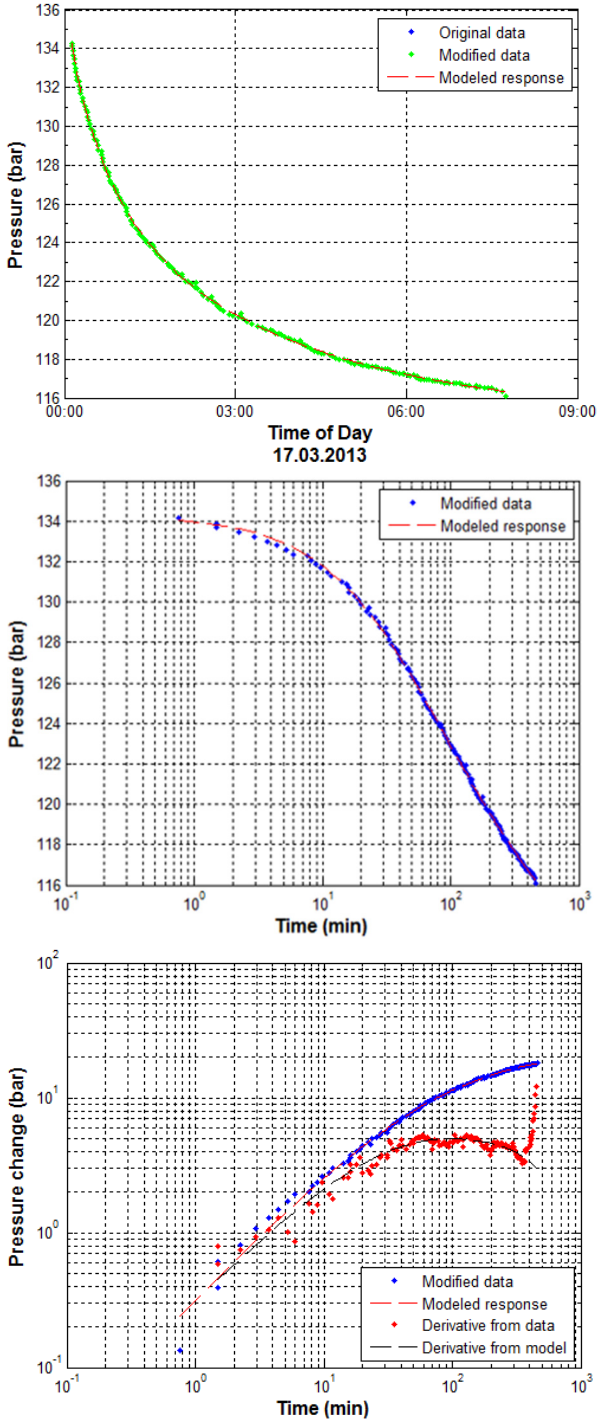

FIGURE 37: Fit between model and collected data in linear, semi-log and log-log scale for step number 5 for Well OW-803

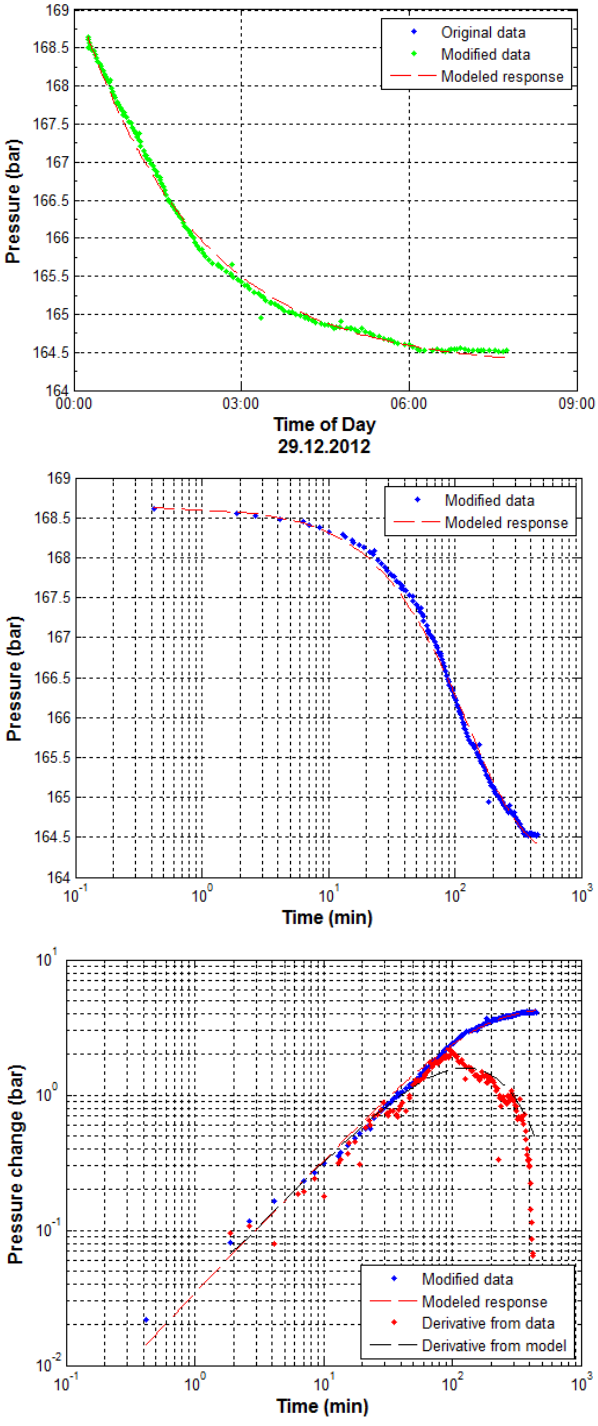

FIGURE 38: Fit between model and collected data in linear, semi-log and log-log scale for step number 4 for Well OW-804

Well OW-804A. Of the four injection steps considered for analysis, the fourth step fitted best to a homogeneous, constant pressure and constant skin with wellbore storage reservoir model. The step returned an injectivity index of 7.23 l/s bar and effective permeability of 1.44 x 10^{-14} m^2. Figure 39 shows the fit obtained for step 4.

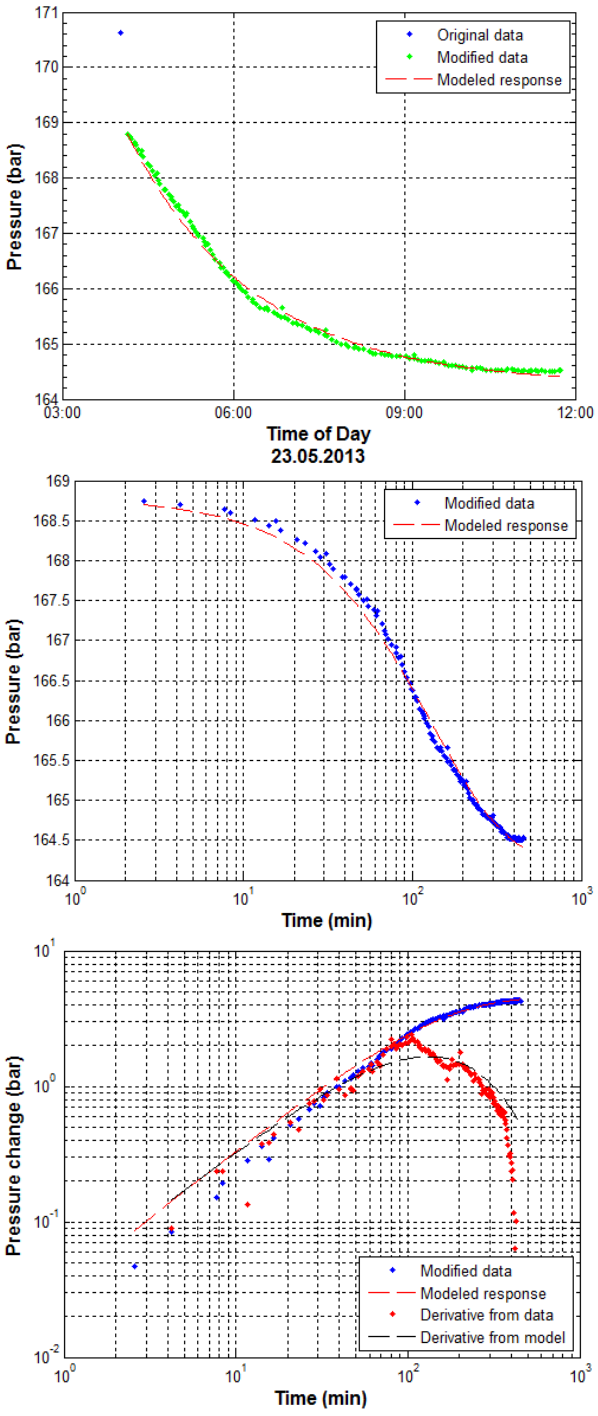

FIGURE 39: Fit between model and collected data in linear, semi-log and log-log scale for step number 4 for Well OW-804A

5. CONCEPTUAL MODEL OF THE FIELD

Grant and Bixley (2011) defined conceptual models as descriptive models of geothermal systems incorporating, and unifying the essential parts of physical features of the system. A conceptual basis is constructed by unified interpretation of data available for a particular field. Incorporation of ideas and viewpoints from various disciplines and expertise are essential in this task. Variable datasets are used in the construction of these models and depend on the phase of development and, therefore, the amount of data available. Fields under exploration rarely have any datasets beyond surface geo-scientific data. In the case of fields that have some or many drill-holes, conceptual models involve the interpretation of a lot more data and are, therefore, considerably more detailed.

The Olkaria geothermal field has been studied extensively over the decades. New information is increasingly acquired with drilling of additional and deeper wells, all of which have dramatically increased knowledge of the system. Down-hole data is of paramount importance in providing calibrations to models developed earlier with little or no information about the different sectors of the field, its geometry, nature and boundaries. The Olkaria conceptual model proposed by West-JEC (2009) and improved by Mannvit/ÍSOR/Vatnaskil/Verkís Consortium (2011) describes the heat source of the system as being of magmatic origin lying at shallow (6 km) depth with dyke intrusions which, in turn, are responsible for at least four up flow areas: one below the Olkaria Domes, another below the East field, still another below the Northeast field and a fourth below the West field. Meteoric water from the high rift scarps percolate deep via deep seated faults dipping into the centre of the rift, are heated on their way, and up-well along permeable structures.

A simple localized model of the Olkaria Southeast production field was developed and is presented in Figure 40. The analyses of temperature and pressure data in Sections 3 and 4 of this work were used to construct a conceptual model of the field. Geothermal fluids permeate through the Ololbutot fracture

zone and the NW-SE faults intersecting it, allowing water to percolate deep into the hot crust. The waters are heated, become lighter and flow towards the surface through permeable zones and structures. The greatest and hottest up flow is located near Well OW-802. The up-welled waters reach the impermeable cap rock above it where it is dispersed on either side of the mushroom-shaped upflow.

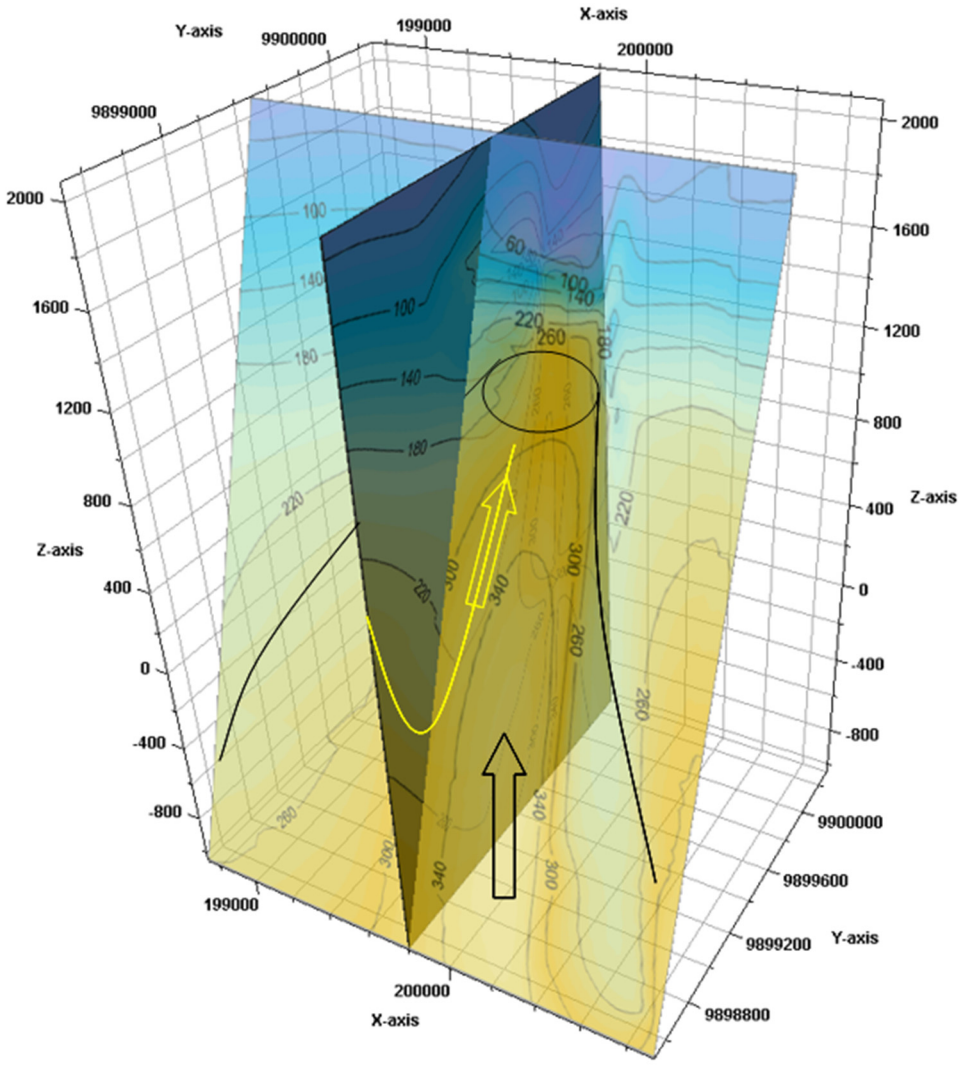

FIGURE 40: Conceptual model of the Olkaria South East production field

6. VOLUMETRIC ASSESSMENT

6.1 Theoretical background

The volumetric assessment method is a static modelling technique mainly used in the mining and petroleum industries. It was more commonly used in geothermal fields in the past than it is today. The Monte Carlo technique is used for repeat multivariable simulation of random variables to generate random inputs from appropriate probability distributions. Essentially, this method approaches the complex question of geothermal resource estimates rather heuristically. For each input variable (except those with lesser uncertainty) in a particular field or situation, computational algorithms are used to sample thousands or more possibilities.

The volumetric assessment is useful in the early stages of development of geothermal fields when little information is available to support more detailed numerical models. In geothermal resource estimation, a resource area is first estimated, then calculations proceed to estimate thermal energy stored in the rock matrix and in the fluid present in rock interstitial spaces. The geometry of the system, its dynamic response to production/injection and hydrologic parameters are not considered. The main benefit of this method, however, is that it offers an early reconnaissance for likely capacity with only limited information.

In the volumetric method, an estimate of the surface area of the resource and its thickness (volume) is required to estimate the thermal heat in place. In many cases, this information is usually deduced from geo-scientific studies of the area. Geophysical surveys, such as MT/TEM, are particularly important in defining resource areas and estimate their probable dimensions before drilling is done. In the absence of these, geological and geochemical data may be used. In drilled prospect areas, better estimates can be obtained from temperature measurements.

The total energy (E_{total}) in the reservoir equals the stored energy in the rock matrix (E_r) and in the pore space volume (E_l) (Equation10). Usable energy is calculated using a reference temperature, T_{ref} referring to the cut off temperature for a specific utilization of the energy.

$$E_{total} = E_r + E_l \tag{10}$$

where

$$E_r = V(1-\phi)\rho_r\beta_r(T - T_{ref})$$

$$E_l = V\phi\,\beta_l\,\rho_l(T - T_{ref})$$

and V =Reservoir volume;
Φ =porosity;
ρ_r = Rock density;
ρ_l = Density water;
β_r = Specific heat capacity of rock;
β_l = Specific heat capacity of water;
T = Reservoir temperature.

Not all available energy is usually accessible. Limits to accessibility are widely variable and may depend on many factors. The accessibility factor, A, is incorporated to discount inaccessible energy from the calculations. The recovery factor, R, defines the proportion of accessible energy that can be technically recovered using available technology. The recoverable energy (E_{rec}) then becomes as shown in Equation 11.

$$E_{rec} = A * R * E_{total} \tag{11}$$

Electrical conversion efficiency, η is then introduced to give an amount of energy that can be converted in a conventional turbine generator.

$$E_e = \eta\, E_{rec}$$

$$P_e = \frac{E_e}{\Delta t}$$

where E_e = Total electrical energy;
P_e = Electrical power potential for generation over time, Δt.

6.2 Model parameters

Surface area. A conclusive anomaly is not apparent in resistivity measurements in a few stations in the area. The surface activity is concentrated along major structures. This is construed to indicate vertical permeability associated with these structures and cannot reliably map out the extent of a viable high temperature resource. It is, however, clear that the up flow zone elongates at least 2-3km (profile 3) and is not more than 750 m thick (profile 2); an area of 2 km^2 is a reasonable lower estimate of proven steam resources. The fact that the temperature diminishes away from the present up flow area indicates that its extent is probably quite limited. In the absence of localized heat sources, the system is expected to be quite narrow with structures being the most important controls. The upper limit is taken to be 6 km^2 which is a guess between the proven resource and the total area available for exploitation.

Thickness. The reservoir is located not less than 1000 m depth. Most of the wells in this area are cased at about 700 m depths; therefore, the maximum production depth is only 2300 m in the deepest well. It is evident that some potentially productive aquifers were already cased off. The bottom of the reservoir has not yet been reached. It was, therefore, decided to take a thickness of 2500 m to represent the upper boundary and 1000 m should reflect the least thickness. It is clear however that the likely thicknesses are closer to the upper limit.

Temperature. Reservoir temperatures taken were between 240 and 360°C. A limit of 240°C was taken as wells this deep may not sustain discharge below this temperature. The choice of this temperature was influenced by recent observations in the marginal wells located in Domes field. It is expected that well discharges are likely to produce fluids at an average of 260°C. The rejection temperature is set at flashing conditions commonly adopted for condensing plants at Olkaria.

Recovery factor. A higher recovery factor was selected, based on the determination of the likely resource area. Since the proven resource area was considered, it is reasonable to elevate the recovery factor. High permeability is observed in this field and, therefore, a higher energy recovery is further justified.

6.3 Monte Carlo simulation

Table 3 summarises the input parameters for the Monte Carlo simulation while the results of simulations for the above input are presented in Table 4. The production capacity of the field is estimated at 42 MWe. Frequency distribution for electrical power potential shows a mean of 45 MWe. 10% of the cumulative probability predicts a 23 MWe output while 90% on the other hand predicts an output of 73 MWe (Figure 41). Sarmiento and Steingrímsson (2011) presented the proposition that 90% of the outcomes represent the maximum possible outcome inclusive of proven, probable and possible resource, while the 10% marker represents the proven resources only.

TABLE 3: Summarized input parameter estimates for Monte Carlo simulation

Input variable	Units	Minimum	Most likely	Maximum	Distribution
Surface area	(km^2)	2	3	6	Triangle
Thickness	(m)	1000	2500	2500	Triangle
Rock density	(kg/m^3)		2700		Fixed
Porosity	(%)	8	--	12	Uniform
Rock specific heat	(J/kg°C)		950		Fixed
Temperature	(°C)	240	260	360	Triangle
Fluid density	(kg/m^3)		900		Fixed
Fluid specific heat	(J/kg°C)		4200		Fixed
Recovery factor	(%)	5	15	20	Triangle
Conversion efficiency	(%)		12		Fixed
Plant life	(years)		30		Fixed
Rejection temperature	(°C)		150		Fixed

TABLE 4: Result of Monte Carlo simulation

Parameter	Units	Result
Most likely estimate		
Energy in place	(TJ)	2216
Total recoverable	(TJ)	332.5
Monte Carlo simulation		
Median electrical power	MWe	42
Mean electrical power	MWe	45
Standard deviation	MWe	20
90% above *(proven)*	MWe	23
90% below *(max. possible)*	MWe	73

7. NUMERICAL MODEL

7.1 Background

Numerical models are distributed models, where many variables are simulated to understand the dynamic nature of systems. By simulating the long term response of fields to exploitation, the models can be a very reliable means for modelling geothermal systems.

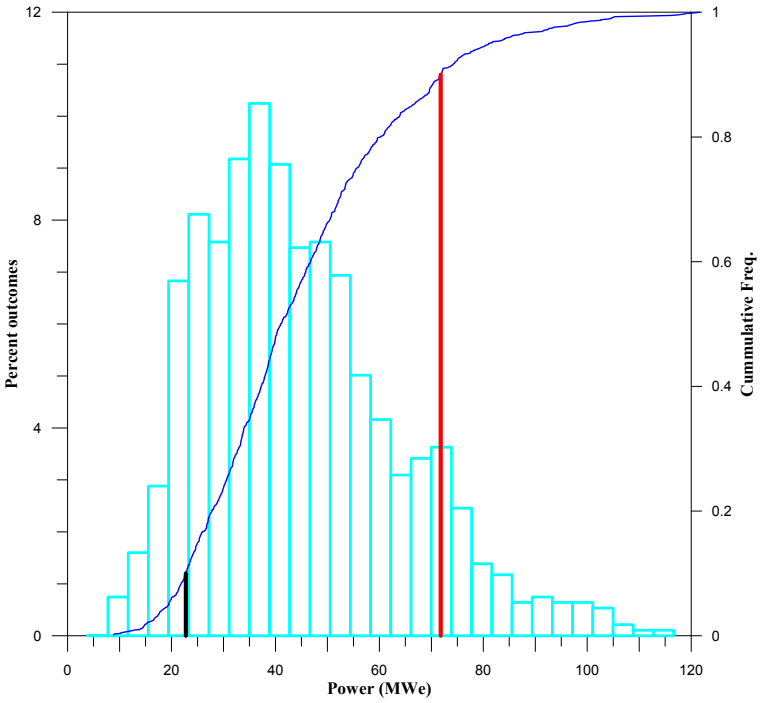

FIGURE 41: Probability distribution and cumulative probability for power output

In numerical models, a conceptual model is relied upon to offer a general understanding of the nature, geometry and size of the system in question. It is important for this conceptual model to sufficiently incorporate all information, usually in many bits and pieces, as presented by various professional disciplines working in the field. The challenge is usually to unify the basic concepts into one single coherent understanding of the field. Each information-set may be found to be extremely important in providing constraints to numerical models. With a qualitative model, largely descriptive, the task and challenge of modelling is henceforth to transform this understanding into a mathematical model which is as close to reality as possible. It is seldom possible to describe the many minor details put into these models, but the main concepts are largely the target of this exercise.

A natural state model is developed to simulate the conditions prevailing in an area or reservoir before exploitation commences. Primary variables to fit into this simulation are the formation temperature and initial pressure data which are estimated from available temperature and pressure measurements. These data can sufficiently describe the important physical state qualities necessary for describing mass and energy fluxes and the balance in the reservoir. Variable data sets may be used here, as well, such as the

distribution of permeability in the reservoir. Boundary conditions are described based on well test data and geological information.

Exploited state models are developed for the field by matching a lot more datasets collected during the historical evolution of the field under exploitation. Often, monitoring reservoirs under exploitation involves the collection of data such as total mass extracted/injected, pressure changes, enthalpy and chemical changes, well deliverability and so on. Data of this kind is simulated and the model is calibrated to match observed parameter trends.

The TOUGH2 and iTOUGH2 codes are examples of numerical modelling codes available commercially. The code solves mass and energy balance equations that describe multiphase flow in multi-component systems (Equation 12). In TOUGH2 (Pruess et al., 1999), appropriate governing state equations of mass and heat transport are discretised by the integral finite difference method and are then solved between consecutive time steps using the Newton-Raphson iteration:

$$\frac{d}{dt}\int_{V_n} M^k \, d\,V_n = \int_{\Gamma_n} F^k \bullet n \, dV\Gamma_n + \int_{V_n} q^k \, d\,V_n \tag{12}$$

where the first term describes the mass and heat accumulation in sub-volume V_n; the second term describes the mass and heat fluxes through the surfaces of the sub-volume V_n; and the last term describes the sources and sinks of mass and heat in the system.

7.2 The computational grid

A TOUGH2 model consists of a number of elements connected to each other in a grid. The described connections between the different elements in space are referred to as a grid. A simple grid was constructed for the OSEPF, containing 1984 elements divided into 8 layers. The stratigraphic layers taken were construed to signify a reasonable distribution of permeability and heat flow. Five different rock types were assigned to the layers. Figure 42 shows the general set up of the grid.

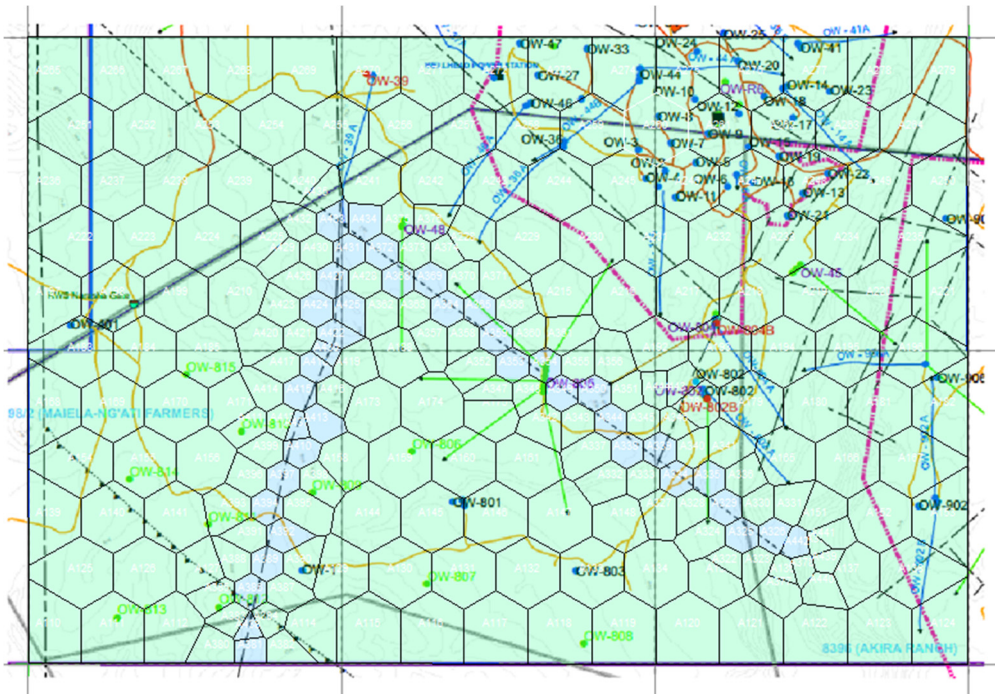

FIGURE 42: The computational grid

7.3 Initial conditions

Initial conditions were calculated for the permeability and heat conductivity allowed for each domain. Simulations were then run to obtain steady state conditions for each element. Initial temperature and pressure conditions observed in well measurements were matched quite closely in this model. Layer A (topmost layer) was initially assigned a temperature of 19.1°C and pressure 5 bar; based on a uniform thermal gradient of 80°C/km, temperature and pressure were assigned to all other layers as shown in Figure 43.

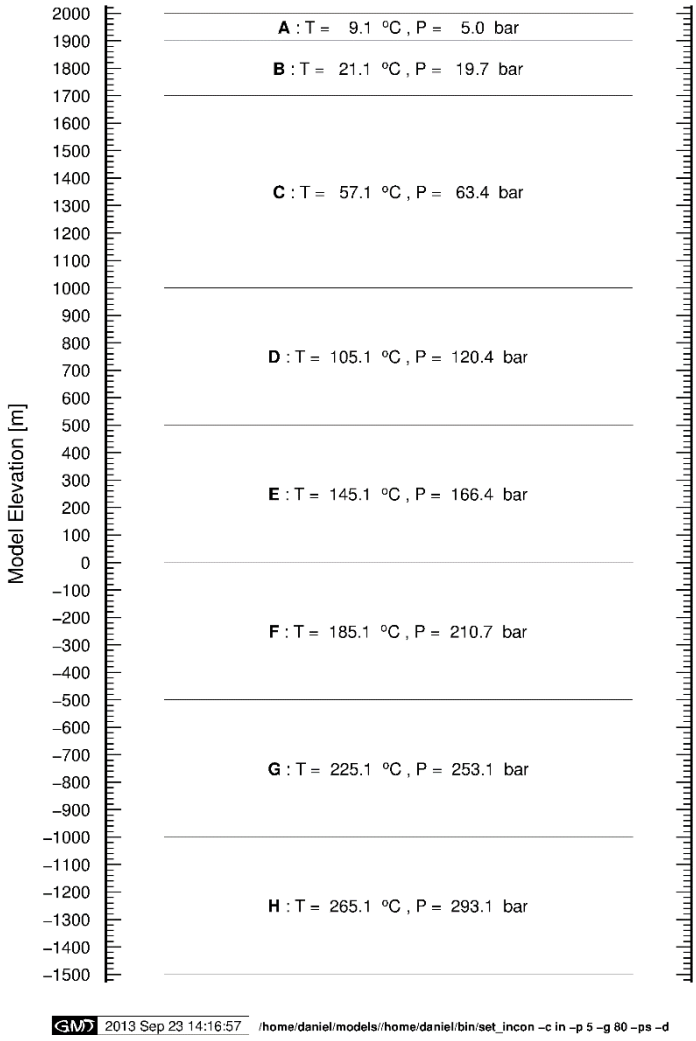

FIGURE 43: Vertical section of the grid showing initial conditions for each layer

7.4 Natural state model

Fluid sources are located in elements in the vicinity of established intersecting structures known to control fluid movements. Mass sources are assigned strengths of between 5-10 kg/s and steady state conditions are calculated where changes in the primary variables are small on the time-scale of several thousand years. Fumarolic activity located in the vicinity of Ololbutot fault to the southeast margin of the field was simulated with a mass sink located in the vicinity of Well OW-1, discharging at -0.0001 kg/s at 2500 kJ/kg. The temperature distribution at depth was matched to the key qualities evaluated in the preceding analysis of pressure and temperature by experimenting with different values for permeability and heat inflow to the system. The reservoir cap was set at about 1000 m a.s.l., where onset of convection was observed. The convective temperatures varied, relative to the well location with respect to the centre of the upflow. Well OW-802, for example, showed convection at about 320°C, while Well OW-804 showed convection at 280°C. On the other hand, Well OW-801, which is located outside this upflow, only reached around 200°C.

An equilibrated model returned the conditions shown in Figure 44 for element A178, located in the vicinity of Well OW-804, element A217 located near Well OW-802, and element A146 which is located near Well OW-801.

Figure 45 shows the modelled temperature distribution for Layer F (sea-level). High-temperature spots are seen in the northeast margins of the field where a NNE-SSW trending anomaly is mapped.

Minor hot zones are also shown to exist in the northwest part of the field, aligned N-S and at the southwest margins. The fluid in this part of the field is associated with the Suswa fault zone and the ring fracture inferred by its close proximity.

8. CONCLUSIONS AND RECOMMENDATIONS

The Olkaria Southeast production field consists of an upflow zone located beneath Well OW-802, which domes to shallow depths at high temperatures and is aligned in a NE-SW fashion. The system is narrow and is highly structurally controlled. The region west of Well OW-803 is shown to be cooling and Wells OW-801 and OW-1 are outside the high-temperature geothermal system.

The reservoir is a homogeneous one with constant pressure boundaries, interpreted to be sustained by recharge from the main structures in the field. Contrary to earlier hypotheses, the geothermal system is not sustained by outflow from the Olkaria East field. On the contrary, it consists of an independent hydrological system controlled mainly from fluid moving from the south northwards, with NW-SE trending structure-dominated fluid movement at depths.

No localized and independent magmatic heat sources were interpreted for this system, but rather were associated with similar magma heat under Olkaria East field. Fluids travelling in the fractures present in the field encounter great heat at depth in the vicinity of the field and upwell at the intersections of grid faults located in the area. The hotter fluids are associated with the NW-SE trending structures passing through Ololbutot lava flow and cool away from it as permeability decreases. Cooler fluid is present in the NE-SW fault intersected by Wells OW-802A and OW-804A but contributes to significant convective zones in these wells.

Plausible drilling targets are along the NW-SE trending faults. This work shows another possible drilling target in the southwest margin of the field, immediately west of the Ololbutot fault. This location is thought to contain hot fluids associated with the Suswa fault zone and the ring fracture.

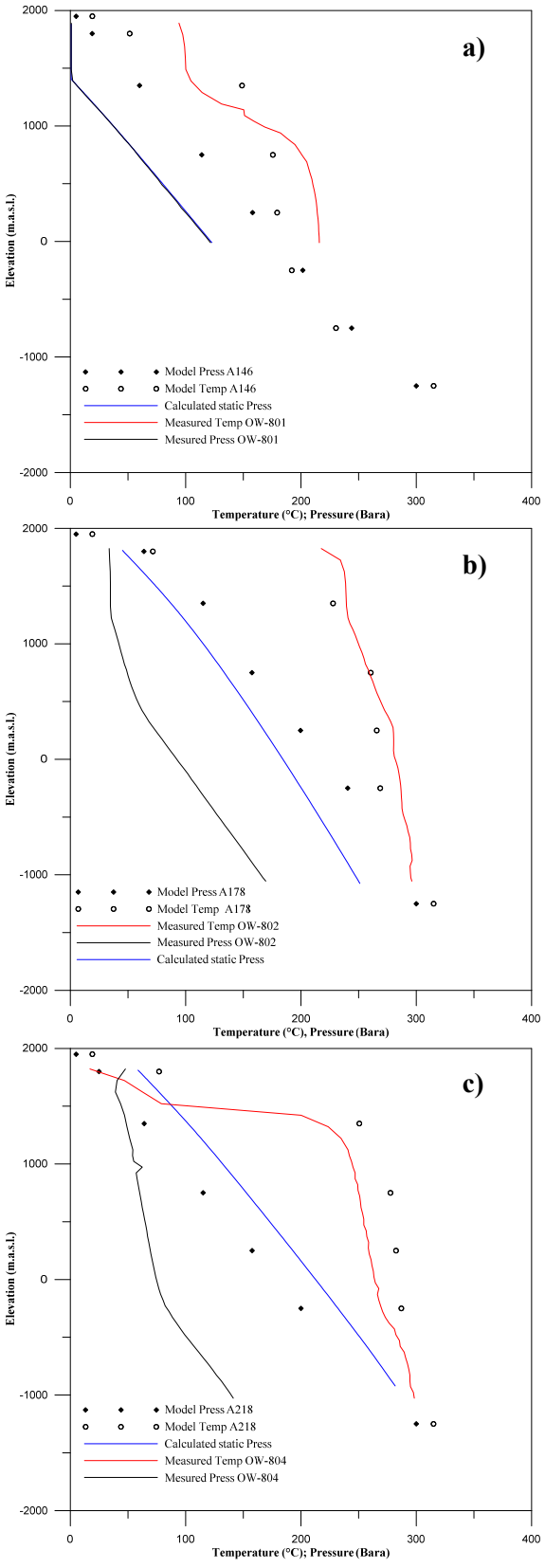

FIGURE 44: Match between well temperatures and pressure and vertical column through elements A146 (a), A178 b), and A218 (c) in the model

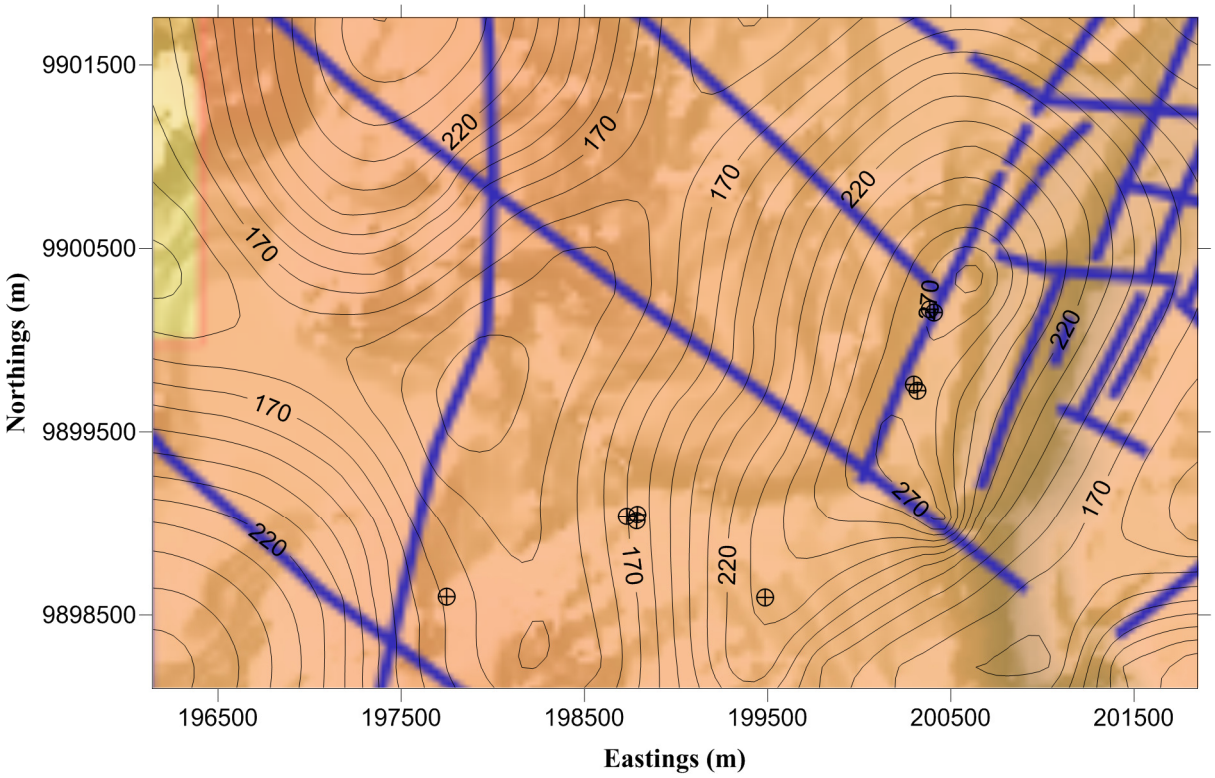

FIGURE 45: Model temperature contours at Layer F (sea level)

REFERENCES

Albright, J.N., 1976: A new and more accurate method for the direct measurement of earth temperature gradients in deep boreholes. *Proceedings of the 2nd United Nations Symposium on the Development and Use of Geothermal Resources, San Francisco,* 847-851.

Arason, Th., Björnsson, G., Axelsson, G., Bjarnason, J.Ö., and Helgason, P., 2004: *ICEBOX – geothermal reservoir engineering software for Windows. A user's manual.* ISOR – Iceland GeoSurvey, Reykjavík, report 2004/014, 80 pp.

Axelsson, G., and Gunnlaugsson, E., (convenors) 2000: *Long-term monitoring of high and low enthalpy fields under exploitation*. World Geothermal Congress 2000, Short Course, Kokonoe, Kyushu district, Japan, 226pp.

Björnsson, G., 1987: *A multi-feedzone geothermal wellbore simulator*. Lawrence Berkeley Laboratory, report LBL-23546, 8-19.

Brown, P.R.L., 1978: Hydrothermal alteration in active geothermal fields. *Annual Review in Earth and Planetary Sciences, 6,* 229-250.

Brown, P.R.L., 1984: Subsurface stratigraphy and alteration of the Eastern section of the Olkaria geothermal field, Kenya. *Proceedings of the 6th New Zealand Geothermal Workshop, University of Auckland, NZ,* 33-42.

Clarke, M.C.G., Woodhall, D.G., Allen, D., and Darling, G., 1990: *Geological, volcanological and hydrogeological controls of the occurrence of geothermal activity in the area surrounding Lake Naivasha, Kenya*. Ministry of Energy, Kenya and British Geological Survey, 138 pp.

Dowdle, W.L., and Cobb, W.M., 1975: Static formation temperature from well logs – an empirical method. *J. Petrol. Tech., 27,* 1326-1330.

Grant, M.A., Donaldson, I.G., and Bixley, P.F., 1982: *Geothermal reservoir engineering*. Academic Press, New York, 369 pp.

Grant, M.A. and Bixley, P.F., 2011: *Geothermal reservoir engineering* (2nd ed.). Academic press, Burlington, USA, 359pp.

Horne, R.N., 1995: *Modern well test analysis, a computer aided approach* (2nd ed.). Petroway, Inc., USA, 257 pp.

Júlíusson, E., Grétarsson, G., Jónsson, P., 2007: *Well Tester 1.0b. User´s guide*. ÍSOR – IcelandGeoSurvey, report 2008/063, 26 pp.

Mannvit/ÍSOR/Vatnaskil/Verkís Consortium, 2011: *Revision of the conceptual model of the Greater Olkaria geothermal system – Phase I.* Mannvit/ÍSOR/Vatnaskil/Verkís, Reykjavík, report, 100 pp.

Muchemi, G.G., 1998: Geothermal exploration in the Kenyan rift. In: Georgsson, L.S. (ed.), *Geothermal training in Iceland, 20th Anniversary Workshop 1998*. UNU-GTP, Iceland, 121-130.

Muchemi, G.G., 1999: *Conceptualised model of the Olkaria geothermal field.* The Kenya Electricity Generating Company, Ltd., internal report, 46 pp.

Omenda, P.A., 1998: *The geology and structural controls of the Olkaria geothermal system, Kenya.Geothermics, 27-1*, 55-74.

Orkiszewski, J., 1967: Predicting two-phase pressure drop in vertical pipe, *J. Petrol. Technol., 19*, 829-838.

Ouma, P.A., 2009: Geothermal exploration and development of the Olkaria geothermal field. *Paper presented "Short Course IV on Exploration for Geothermal Resources", organized by UNU-GTP, GDC and KenGen, at Lake Naivasha, Kenya*, 16 pp.

Pruess, K., Oldenburg, C., and Moridis, G., 1999: *TOUGH2, user´s guidance version 2.0.* Lawrence Berkeley National Laboratory, 197 pp.

Reyes, A.G., 2000: *Petrology and mineral alteration in hydrothermal systems: from diagenesis to volcanic catastrophes.* UNU-GTP, Iceland, report 18-1998, 77 pp.

Sarmiento, Z.F., and Steingrímsson, B., 2011: Resource assessment I: introduction and volumetric assessment. *Paper presented at "Short Course on Geothermal Drilling, Resource Development and Power Plants, organized by UNU-GTP and LaGeo, in Santa Tecla, El Salvador*, 15 pp.

Simiyu, S.M., and Keller, G.R., 1999: Seismic monitoring of the Olkaria geothermal area, Kenya Rift Valley. *J. Volcanology & Geothermal Research, 95*, 197-208.

Takai, K., Hyodo, M., and Takasugi, S., 1994: Estimation of equilibrium formation temperature by curve-fitting method and its problems. *Proceedings of the 19th Workshop on Geothermal Reservoir Engineering. Stanford University, Stanford, Ca*, 65-73.

West JEC, 2009: *Olkaria optimization study (phase II). Final report*. West JEC, report made for KenGen, 64pp.